14P

1000820

RECENT PROGRESS IN THE REMOTE DETECTION OF VAPOURS AND GASEOUS POLLUTANTS

By

A. J. Moffat and A. R. Barringer
Barringer Research Limited
Rexdale, Ontario, Canada

ABSTRACT

Work has been continuing on the correlation spectrometry techniques described at previous Remote Sensing Symposiums. Advances in the techniques are described which enable accurate quantitative measurements of diffused atmospheric gases to be made using controlled light sources, accurate quantitative measurements of gas clouds relative to background using solar illumination and semi-quantitation measurements of well diffused atmospheric gases using solar illumination. Specific applications of these techniques are described including preliminary results of a high altitude balloon experiment designed to test the feasibility of measuring pollution at the earth's surface from high altitude balloons and satellites.

INTRODUCTION

The application of state-of-art remote sensors to the detection and measurement of targets in or through the earth's atmosphere, invariably involves consideration of the properties of the atmosphere itself. If the target is a cloud of gas immersed in the atmosphere then the problem is further complicated by the dynamic behaviour of the target. The optical properties of a gas target may not only be subject to change due to molecular diffusion and turbulent mixing with the ambient air, but it may also be subject to both chemical and physical transitions. Investigators concerned with the measurement of trace gases in the atmosphere using active long path electro-optical devices for example, may find the lower level of detectibility is limited by atmospheric turbidity, scintillation, image-dancing and interference from scattered solar flux. In the remote measurement of sulphur dioxide plumes at the top of a chimney or stack, accuracy is determined by turbulence at the stack exit and optical scattering in the atmosphere between the plume and the sensor. From a high flying aircraft or satellite, the accurate determination of gas concentration in the atmosphere presupposes a knowledge of the absorption and scattering properties of the atmosphere, reflectance properties of the ground and vertical extent of the gas target. For measurement of the mass transport of gases in the atmosphere, a knowledge of wind velocity as a function of altitude is also required.

The purpose of this paper is to review recent advances in design of a particular type of correlation spectrometer and specifically to present preliminary results of a high altitude balloon experiment over Chicago.

THE CORRELATION SPECTROMETER

The principle of correlation spectrometry and its application to the remote sensing of atmospheric gases has been adequately described in the literature (1-6). The emphasis here, will be on the extention of the refractor plate/tuning fork modulation method to include a relatively slow sine wave oscillation of the target spectrum. The superposition of two spatial oscillations of the spectrum relative to the correlation mask has greatly simplified the correlation spectrometer approach to long path measurements using artificial light source and to airborne measurements using solar illumination. The technique also appears suitable for spacecraft applications.

35P

Figure 1 shows the absorption spectra of three gases currently under active investigations as remote sensor targets. The upper trace shows the SO_2 band structure extending from 2850 Å to about 3150 Å. The set of bands illustrated above the trace (wavelengths longer than 3000 Å) are those used for passive remote sensing i.e. solar illumination. For active systems where energy is available at all wavelengths of interest, the mask may contain as many as 10 slits and be centered on the most intense band. The absorption bands presently used for NO_2 and I_2 sensing are similarly shown. Here again the choice of spectral bands and design of the mask will depend on the light source characteristics. Mask optimization for a given application is an automated mathematical process in which the response of a computerized model of the correlation spectrometer is examined over the full range of anticipated light source spectral characteristics, target gas concentration and possible interfering spectra for a given mask design. Experience to date has shown excellent agreement between theoretical performance predicted by computer modelling and actual performance from working prototypes.

Figure 2 illustrates the basic correlation spectrometer. The field-defining foreoptics is comprized of M_1 and M_2, a cylindrical lens and the entrance slit. The spectrometer itself, is an F 3.6 Ebert-Fastie configuration of 1/4 meter focal length. The correlation mask is stationary and the spectrum of the incident light is spatially modulated relative to the mask by means of the fork-driven quartz refractor plates. The fork is driven at 100 hertz. A high-gain photo-multiplier tube is used to detect the mask/spectrum correlation function. This is followed by a FET pre-amplifier, the output of which is a series of unidirectional pulses produced by the spectrum moving in square wave fashion from one discrete position to a second discrete position and back again. Figure 3 illustrates the arrangement of spectrum and slits in the plane of the exit mask. Considering, for simplicity, only one slit in position 2, then the modulation ratio is:

$$M = \frac{I_0 e^{-a_1 cl} - I_0 e^{-a_2 cl}}{I_0 e^{-a_1 cl}} \quad (1)$$

where I_0 = incident light

a_1 = average minimum absorption coefficient across the slit

a_2 = average maximum absorption coefficient across the slit

c = concentration

l = pathlength

and $$M = 1 - \frac{e^{-a_2 cl}}{e^{-a_1 cl}} \quad (2)$$

or $$M = 1 - e^{-(a_2 - a_1)cl} \quad (3)$$

From equation (2) it is easily seen that the instrument simply measures the ratio of energy contained in the spectrum viewed by the slit. Operation of a spectrometer using a single slit is often very useful in the study of light sources and possible competing absorbers since it produces, in effect, a low resolution first derivative of the spectrum under observation. For near real-time detection purposes however, it would suffer from low energy throughput and low specificity. The number of slits used in remote sensor masks may vary from 5 to more than 10 depending on the application. A typical response curve as a function of target gas in ppm-meters is shown in Figure 3.

Referring again to slit array in Figure 3, if the spectrum is now considered to move to the left while the slit is oscillating back and forth between positions 1 and 2, then it is obvious that the modulation ratio will swing through positive and negative values in a periodic fashion. This is the basis of the instrument operation to be described.

REMOTE SENSING WITH ARTIFICIAL SOURCE

Use of an artificial light source in remote sensing has a distinct advantage over the solar source in that its characteristics are controlled and well defined. Also for the investigation of dispersed gases in the atmosphere, the long path lengths available permit accurate quantitative measurements of very low average concentrations. Figure 4 shows the typical recordings of an SO_2 correlation spectrometer obtained using a 3200 °K quartz iodine lamp. The secondary spectrum motion was achieved by oscillations of the grating and the traces were produced while slowly scanning the grating in one direction over four bandheads. Each positive or negative peak represents a condition

of maximum correlation of the slits in the mask, with the absorption bands in the spectrum. The magnitude of the peak-to-peak deflection is a function of the difference in the energy content of the peaks and troughs in the spectrum which of course is a function of the gas concentration and the optical path length as shown in the Figure. These recordings were obtained using a one-meter test cell. In practice, only one peak-to-peak correlation cycle is used, as indicated by the darkened trace, and the grating is oscillated back and forth over the chosen wavelength interval. The final trace shows the typical double peak characteristic obtained as the cell was being pumped down. The light beam from the lamp used for these particular recordings was chopped at 2.2 K hertz. The use of a chopped source and bandpass filtering in the sensor electronics enables the sensor to discriminate against solar illumination.

Figure 5 shows similar recordings for an NO_2 long path system. The trace in the upper left of Figure 5 is a multiband scan in one direction. The traces at lower left were obtained with a one hundred fold increase in gain. At zero gas concentration the base line shows a distortion of 1 ppm-meter peak-to-peak. Note however that the photon noise is still very low and since the base line profile remains virtually constant over long periods of time it is possible to measure very low gas burdens by observing departures from this profile. By making refinements to the technique, it should be possible to routinely measure average gas concentrations substantially below 1 ppb in a path length of 1000 meters.

Figure 6 shows the sensor response over a range of 0-1000 ppm-meters for both NO_2 and SO_2. Ordinate values are the peak-to-peak values obtained from figure 4 and 5. Note that in both cases the response is essentially linear out to about 600 ppm-m i.e. 1 ppm in 600 meters. Tests of the above long-path sensor, using both quartz iodine and chopped xenon arc sources have been carried out in several urban locations including Toronto, Ontario for SO_2 and Pomona, California for NO_2. Operation over pathlengths exceeding 1000 meters was achieved with very encouraging agreement with simultaneous wet chemistry measurements.

Figure 7 shows a typical recording from a sensor operating over a pathlength of 930 meters. A chopped xenon arc source was used in this case. The very large changes in amplitude were caused by one or more plumes from local industry inundating the test area.

The maximum pathlength attainable is dependent on the relative magnitude of the solar component received at the sensor and the severity of atmosphere-induced fluctuations in the chopped (Xenon) component. Investigations to date indicate that both image dancing (fluctuations in angle of arrival of wave front) and amplitude scintillation (intensity fluctuations) play a part in atmosphere induced noise and both are dependent on the dynamic state of the atmosphere i.e. on the degree of atmospheric mixing or turbulence. The automatic gain control circuit used in the sensor, samples the light level once every fork period i.e. every 10 msecs with the result that intensity fluctuations exceeding 30% can be tolerated before accuracy is impaired.

At present, operation beyond 1000 meters is possible only if precautions are taken to limit the solar component. Forward scattering of sun light in a typical urban atmosphere is such that large errors will result if the sensor is so oriented that the sun can approach within 20° of its line of sight.

Refinements in instrument design currently underway are expected to improve both scintillation and solar rejection characteristics to the point where operation over pathlengths beyond 1000 meters will be possible.

REMOTE SENSING USING SOLAR ILLUMINATION

Use of the solar source for remote sensing with a correlation spectrometer requires detailed knowledge of the solar spectral distribution. The presence of sharp irregularities in the source continuum will produce characteristic distortion in the instrument output. Figure 8 shows typical output profiles in the ultra-violet. These traces were obtained with a 6 slit SO_2 mask designed to cover the range 3000 to 3150 Å but not optimized for Fraunhoffer rejection. Note the very pronounced sky signature as compared with the zero correlation output using the quartz iodine. Investigations to date indicate that correlation with Fraunhoffer structure in the solar spectra is the primary reason for these distortions and these appear to be borne out by the high degree of repeatibility of sky profile regardless of the time or geographic location. Experience to date indicates that reliable measurements of target gas concentrations can be made by using the sky profile as a reference and observing departures from it due to absorption by the target gas. The lower trace shows the effect of superimposing a strong SO_2 profile. It is evident then that it should be possible to extract the SO_2 component from any given target signature by cross correlation with an SO_2 reference waveform.

Figure 9 further illustrates the effect of increasing SO_2 concentrations. The inverval bounded by the dotted lines is the scanning interval chosen for a high altitude balloon experiment because of the relatively high light level available and the relative ease of data interpretation.

Figure 10 shows similar profiles for NO_2. These were obtained using a 5 slit mask covering the range 4300 to 4500 Å. Fraunhoffer lines are particularly strong in this region and the Fraunhoffer correlations coincide exactly with those for NO_2. The method of measurement in this case is simply to observe the increase in peak-to-peak amplitude caused by NO_2 absorption. The dotted lines again indicate the inverval used for the balloon experiment.

PLUME MEASUREMENTS

The measurement of concentration of a target gas in the atmosphere is complicated by the requirement for determination of pathlength and the effect of scattering between the gas cloud and the sensor.

For measurements of effluent from the top of a chimney or stack however, the plume at the stack exit is usually reasonably well defined and scattering can be taken into account by taking several measurements at different ranges and projecting the resulting curve back to the point of emission. Figure 11 is typical of data obtained when measuring stack SO_2 effluent and illustrates the loss of signal as a function of range due to atmospheric scattering between the stack and the sensor. Visibility at the time these data were taken was 16.4 kilometers. The effect of scattering is of course more pronounced as visibility is lowered and the range at which reliable measurements can be made is reduced. Details of the method are treated fully in reference (4) and will not be considered here.

REMOTE SENSING FROM SPACE - THE BALLOON EXPERIMENT

On September 3, 1969 a high altitude balloon experiment was performed to test the feasibility of detecting pollutants in the lower atmosphere from a spacecraft. This work was performed under contract to NASA. Management of the balloon system and launch program was the responsibility of the National Centre for Atmospheric Research (NCAR), the balloon system and launch crew were provided by Winzen Research Inc., and the scientific package and sun tracker were the responsibility of Barringer Research Limited. The balloon was launched from Dowagiac, Michigan and carried SO_2 and NO_2 correlation spectrometers, plus a radiometer, along a curving trajectory over Chicago at an altitude of 35 Km (114,000 ft.). The complete results of the project have not yet been fully evaluated and only a preliminary analysis of the results is presented. The purposes here is to describe the experiments in general terms and to outline some of its salient features.

A prime consideration in the detection of surface pollutants by remote sensing from above the earth's atmosphere is the level of radiant flux emerging from the top of the atmosphere which has been reflected by the earth's surface and its magnitude relative to emerging flux which has not reached the surface but has been reflected or back-scattered by the atmosphere. Figure 12 depicts the mechanisms involved and their influence on the remote sensor measurement. Note that attenuation of ultraviolet radiation occurs primarily by ozone absorption in the upper layer (between 20 and 30 Km) and by scattering in the more dense atmosphere between the ozone layer and the earth's surface. Note also that radiant power which has been reflected from the earth's surface and contains the desired gas signature must compete with backscattered flux containing little or no gas signature. This dilution effect is most severe in the ultraviolet and diminishes in severity with increasing wavelength. In addition, the relatively low reflectance of the earth's surface in the ultraviolet further reduces the useful SO_2 signal. Extensive tables exist for determining the flux levels emerging from the top of the atmosphere for various sun angles, molecular and aerosol number densities and ground albedoes (7) but very little theoretical or experimental data exists which accurately describes the properties of a heavily polluted atmosphere over an industrial city. However, extensive tests of an airborne SO_2 remote sensor over industrialized areas (1), (3) have clearly demonstrated a capability for aircraft pollutant monitoring and extrapolation of this performance to a spacecraft has indicated a good probability of success. This has provided the main impetus for the balloon experiment.

Figure 13 shows curves reproduced from the Air Force-Cambridge Handbook (8) of the outgoing flux as a function of wavelength for various surface reflectances. The upper dashed curve is the incident solar flux for the sun at the zenith. Lines A and B indicate the approximate centre wavelength of the SO_2 and NO_2 masks respectively.

The city of Chicago was chosen as the target for the balloon experiment primarily because of its size, pollutant source strength and excellent ground monitoring system. In addition, numerous

small airfields in the South Bend area offered the desired flexibility in launch site selection. An east-to-west trajectory over south-central Chicago at an altitude of 35 Km (≈114,000 ft.) was planned with the balloon scheduled to arrive over the city as close as possible to 12:00 noon solar time.

Figure 14 shows the balloon system configuration. The ladder cable was constructed of 3/16 steel cable with 18" aluminum spacers to provide the stiff coupling to the balloon necessary for the azimuth stabilization system. A solar orientation system designed by the University of Saskatchewan was used to maintain a constant solar heading during float to avoid errors being induced by changes in polarization of the upcoming solar flux.

Figure 15 shows the sensor payload. Both sensors scanned the ground through a common mirror assembly which was driven by a solenoid in bi-stable fashion from a position of vertical line of sight to a position 24° to the anti-solar side. This was done to provide sampling of the atmosphere over two parallel ground tracks approximately 10 miles apart. The bias to the anti-solar side was to take advantage of the reduced backscatter in the anti-solar direction. Spatial resolution was 1° or about 1/2 mile on the ground. Spectral characteristics of the two sensors are as follows:

	SO_2	NO_2
Center Wavelength	3100 Å	4400 Å
Spectral bandwidth	150 Å	200 Å
Grating Scan range	6.2 Å	25 Å
Garting Scan rate	0.2 hz	0.9 hz

A solenoid-driven diffuser plate and quartz iodine light source were provided for calibration purposes. The radiometer is a Barringer Research development and designed to measure contrast ratios of the terrain at wavelengths of 3100 Å and 6000 Å. A detailed discussion of this instrument will not be included here, but briefly and in principle it scanned a small cone around the nadir and generated a high frequency output corresponding to the changes in reflectance plus a larger low frequency and DC component due to atmospheric backscatter. By using the average value of the signal to control an AGC loop, the high frequency output can be made proportional to the apparent contrast changes in the terrain. Then given the average values and variations in reflectance at the two wavelengths, the ratio of apparent and actual contrasts show how the target signal is diluted by backscatter. This instrument performed remarkably well during the flight but considerable work remains to be done in the data reduction.

Figure 16 shows the fully assembled gondola mounted on the launcher undergoing final inspection. The lower second is a crush pad and the sensor compartment is enclosed in foamed urethane panels. The packages on the upper level are telemetry and balloon control units. All data were transmitted to ground via FM/FM telemetry. The sun tracker photocells are mounted on an aluminum pedestal under a circular baffle. This photo was taken only a few moments before launch.

Figure 17 shows the arrangement for a secondary experiment. The purpose of this installation was to measure the SO_2 burden in the atmosphere over Chicago from the ground coincident with the balloon measurements aloft. The remote sensor shown in the figure was adjusted to scan the spectral range identical to that of the balloon unit. By comparing the balloon measurements of SO_2 with that of the ground vehicle, with due consideration for the multi path factor in the balloon results, the best possible measure of dilution can be arrived at.

A balloon launch during August was preferred in order to take advantage of the high sun altitudes and the higher probability of favourable conditions as compared with later in the year. Towards the end of August however, the upper level winds enter the turn-around phase (at Chicago's latitude) and as the speed drops, both the speed and direction become less predictable. From September 1st to October 15th the winds aloft are not generally suitable for balloon experiments. Assuming a launch in August, a launch site was selected at Dowagiac, Michigan and subsequent computed trajectories by NCAR's Palastine computer facility confirmed the choice. With an accumulation of minor delays in the program however, the launch date slipped to September 3rd/69. By August 26th a deteriorating tread in wind conditions had set in. On September 2nd NCAR's studies showed the upper level easterlies were still holding although growing weaker and more variable and that surface conditions over Chicago should be favourable for a launch the following day. The launch took place at 4:55 CST September 3/69 Figure 18 shows the actual balloon trajectory. The dotted track is the station wagon route. The circuitous track of the balloon was completely unexpected although the south-westerly and north-westerly position of the trajectory were anticipated. Unfortunately, heavy cloud covered the early portion of the track, but by 10:15 CST this had given way to scattered to broken cumulous along the trajectory over Chicago. Under the influence of a light

(7 knot) easterly wind and strong inversion conditions the ground level SO_2 levels were somewhat higher than usual as shown by the ground station readings in Figure 19. These values are for 12:15 CST and were obtained from the automated pollution monitoring network of the City of Chicago. The stationwagon followed a route which was intended to approximate the predicted East to West balloon trajectory (as far as Joliet). The stationwagon had reached Joliet when advised of the balloon's change in direction and immediately turned back to intercept the balloon's ground track in the center of Chicago.

Figure 20 shows typical waveforms from the balloon SO_2 sensor. The upper trace is typical of a sky signature with perhaps a small amount of SO_2 present. This was obtained early in the flight (10:00 CST) at a time when substantial cloud cover was still present. The double peak was produced by scanning over the sky profile between the limits indicated by the dotted lines in Figure 9. Filling-in of the trough between the peaks and increase in the peak-to-peak values is indicative of increased SO_2 absorption as shown also in Figure 9. Disregarding dilution, the amount of SO_2 present in the sensors field of view, relative to that in the background (upper) waveforms, is determined by measuring the increase in peak-to-peak amplitude at the grating reversal points, that is at the mid-point of the +ve and -ve swings. The incremental sensitivity of the instrument is given by the increase in the peak-to-peak value using a reference cell of known SO_2 content. The lower trace shows the effect of inserting 55 ppm-meters of SO_2 in the instrument's field of view.

Figure 21 shows typical waveforms from the NO_2 sensor. As mentioned earlier the quantity of NO_2 detected by the instrument is determined by measuring the maximum peak-to-peak amplitude of the waveform. Here again the contribution of an NO_2 cloud is measured relative to a minimum gas waveform obtained at some point in the flight. The abrupt increase in peak-to-peak value evident in Figure 21 is the result of inserting a reference cell of 132 ppm-meters.

Figure 22 shows several samples of the station wagon record. These traces, which read from right to left in time, show a number of extremely large responses obtained as the station wagon passed under SO_2 plumes as it sped along the highway. It should be noted that a remote sensing correlation spectrometer of the type considered here (1° F.O.V.) has inherently greater sensitivity and better resolution in the upward scanning mode as used in ground traverses than in the downward looking mode as used in aircraft and balloons because of the greatly reduced scattering and dilution. In Figure 22 the characteristic double peak does not appear over much of the trace because of the high gas burdens. This effect is also evident in Figure 9.

Figure 23 shows a three-dimensional plot of the SO_2 burden measured by the station wagon. Note that the wagon route crosses the balloon ground track at two points; near ground station No. 23 where the wagon followed a detour to the north of Route 80 on the west bound leg and later the Chicago waterfront where the balloon left Chicago and floated out over the lake. The SO_2 levels were very low from the intersection of Routes 80/294 until the wagon reached a point just west of Joliet. At this point a strong signal (360 ppm-m) of short duration was recorded. A second signal of 725 ppm-m peak value was recorded after turning north on Route 55. From analysis of the wagon positions, chart profiles and wind direction, it was subsequently deduced that the wagon had measured the same plume twice as indicated in Figure 23. The identity of the industry south of Joliet has not yet been determined. The peak ppm-m value of the plume was not reached on the first pass because of the small size of the concentrated plume and the speed of the vehicle. Further north on Route 55 the wagon again recorded a very strong signal. This time the source was identified as the Romeoville Generating Station. This is a very large thermal plant. Its SO_2 emissions are essentially uncontrolled.

As the station wagon approached Chicago a substantial build-up of SO_2 was recorded. The origin of this was not determined but it was possibly due to the Calumet/State Line plume being carried westward by the easterly surface winds. Unfortunately, the major contributors to SO_2 pollution in the Chicago area: the Ridgehead, Crawford and Fisk Generating Stations were all downwind of the wagon route and no plumes were detected.

Figure 24 shows a computerized plot of the balloon SO_2 profile. Note that the SO_2 signals obtained are shown plotted as discrete values on a base line which is the ground track of the remote sensor's field of view when the scanning mirror was in the 24° position. This base line is referred to as the "24° scan line". The gradual convergence of the 24° scan line and the balloon ground track with time is due to the gondola's solar tracking system which maintained the plane of the mirror scan angle in alignment with the sun's azimuth position. Spacing of the data points is irregular because of intermittent cloud cover and a large gap occurs between 1052 and 1200 hours, because of instrument adjustments. Figure 25 shows similar data for the 0° scan line which corresponds to the balloon ground track. The absence of data before 1015 hours was due to heavy cloud cover.

After 1315 hours over the lake, the sky was completely clear of cloud but SO_2 levels were negligible. The build-up of SO_2 over the city is obvious and it is significant that the maximum SO_2 signals recorded by the balloon sensors correspond to the location of maximum surface SO_2 levels as recorded by the ground stations.

The NO_2 profile obtained along the 24° scan line is shown in Figure 26. The reason for the NO_2 data occuring in sets of two is due to time sharing between the zero degree and twenty-four degree scan positions.

The data reduction procedure involved an initial inspection of the analogue waveform to identify calibration periods and mirror positions and to establish the zero gas reference level. The waveform was then digitized and the data reduced from thereon by computer to arrive at ppm-meter values. Another program, individually corrected these values for calibration intervals, and for changing sensor field-of-view position. Using coordinates as a function of time, a Calcomp plotter placed the final ppm-meter values on a hand digitized map of Chicago. The wind data shows surface conditions present at 1215 CST on September 3rd, 1969.

There are voids in the data of Figure 26 again, because of intermittent cloud cover. Maximum values again correlate reasonably well with maximum ground level values.

Figure 27 shows the NO_2 zero degree case. Note that the location of maximum recorded levels of Figure 27 as compared with that of Figure 26 indicates the presence of possibly two separate pollutant clouds, one centered near station 8 and the other near station 24. The former cloud is no doubt the effluent, from the Calumet/State Line generating stations. The combined output of these sources is 80,622 tons of SO_2 annually. The NO_2 or potential NO_2 (NO) output is not known. The origin of the pollutant cloud in the vicinity of station 24 was not determined but its presence was confirmed by the station wagon as shown in Figure 23. Unfortunately, no data were obtained from the balloon over station 24 although some data were obtained somewhat further west as shown in Figure 24.

CONCLUSIONS

This paper has described recent progress in the development of correlation spectrometry techniques as applied to a variety of remote sensing tasks. The major effort which has gone into this work has not been in instrument design so much as it has been in striving to obtain a better understanding of the information derived by such techniques. Qualitative interpretation of correlation spectrometer data is relatively simple and quantitative interpretation of spectrometer data output when using a controlled light source is quite straight forward but accurate absolute quantitative interpretation of correlation spectrometer data using solar illumination requires very precise control of instrument parameters and very careful analysis of the data. Future work in this area, that is, remote sensing using solar illumination, will concentrate on improving the over-all signal-to-noise ratio of the measurement using current instrument configurations. Current status of correlation spectrometry techniques require the independent determination of atmospheric scattering for quantitative remote sensing of atmospheric gases from spacecraft. Consideration is presently being given to the development of techniques which utilize only the ground-reflected radiation and effectively reject the troublesome atmosphere-reflected component.

ACKNOWLEDGEMENTS

The authors gratefully acknowledge the support of the National Air Pollution Control Administration, (NAPCA) DHEW Cincinnati for evaluation of the ground based remote sensor for pollution measurements: the assistance and cooperation of the National Center for Atmospheric Research (NCAR) on the balloon program, the University of Saskatchewan for use of the sun tracker design and technical assistance on the balloon project; the City of Chicago for cooperation and assistance in providing ground data, Environmental Measurements Inc. of San Francisco for conducting the station wagon traverse and last but not least NASA for financial support of the balloon project.

REFERENCES

1. Barringer, A. R., Newbury, B. C., Moffat, A. J. (1968) - Surveillance of Pollution from Airborne and Space Platforms. Fifth Remote Sensing Symposium Ann Arbor, Michigan, April 1968.

2. Williams, D. T., Kolitz, B. C. - Molecular Correlation Spectrometry. Applied Optics, Vol. 7, No. 4, April 1968.

3. Barringer, A. R., - Chemical Analysis by Remote Sensing. The 23rd Annual ISA Instrumentation Automation Conference, October 1968.

4. Moffat, A. J., Robbins, J. R., Watts, R. M., Millan, M. - The Applications of Optical Correlation Techniques to the In-Stack Measurement of SO_2 Using Incandescent Light Sources and the Remote Sensing of SO_2 Plumes Using Sky Light. Symposium on Advances in Instrumentation for Air Pollution Control, NAPCA, Cincinnati, Ohio, June 21, 1969.

5. Moffat, A. J., Robbins, J. R., Barringer, A. R., - Electro-Optical Sensing of Environmental Pollutants. 158th ACS Meeting, Division of Industrial and Engineering Chemistry, New York City, September 12th, 1969.

6. Millan, M. M., Townsend, S. J., Davies, J. H., - Study of the Barringer Remote Sensor, University of Toronto Institute for Aerospace Studies, Report No. 146, October 1969.

7. Dave, J. V., Furukawa, P. M., - Scattered Radiation in the Ozone Absorption Bands at Selected Levels of a Terrestrial Rayleigh Atmosphere. The American Meteorlogical Society, Meteorlogical Monograph Volume 7, January 1966, No. 29.

8. Air Force Cambridge Research Laboratories - Handbook of Geophysics and Space Environments, McGraw-Hill, 1965.

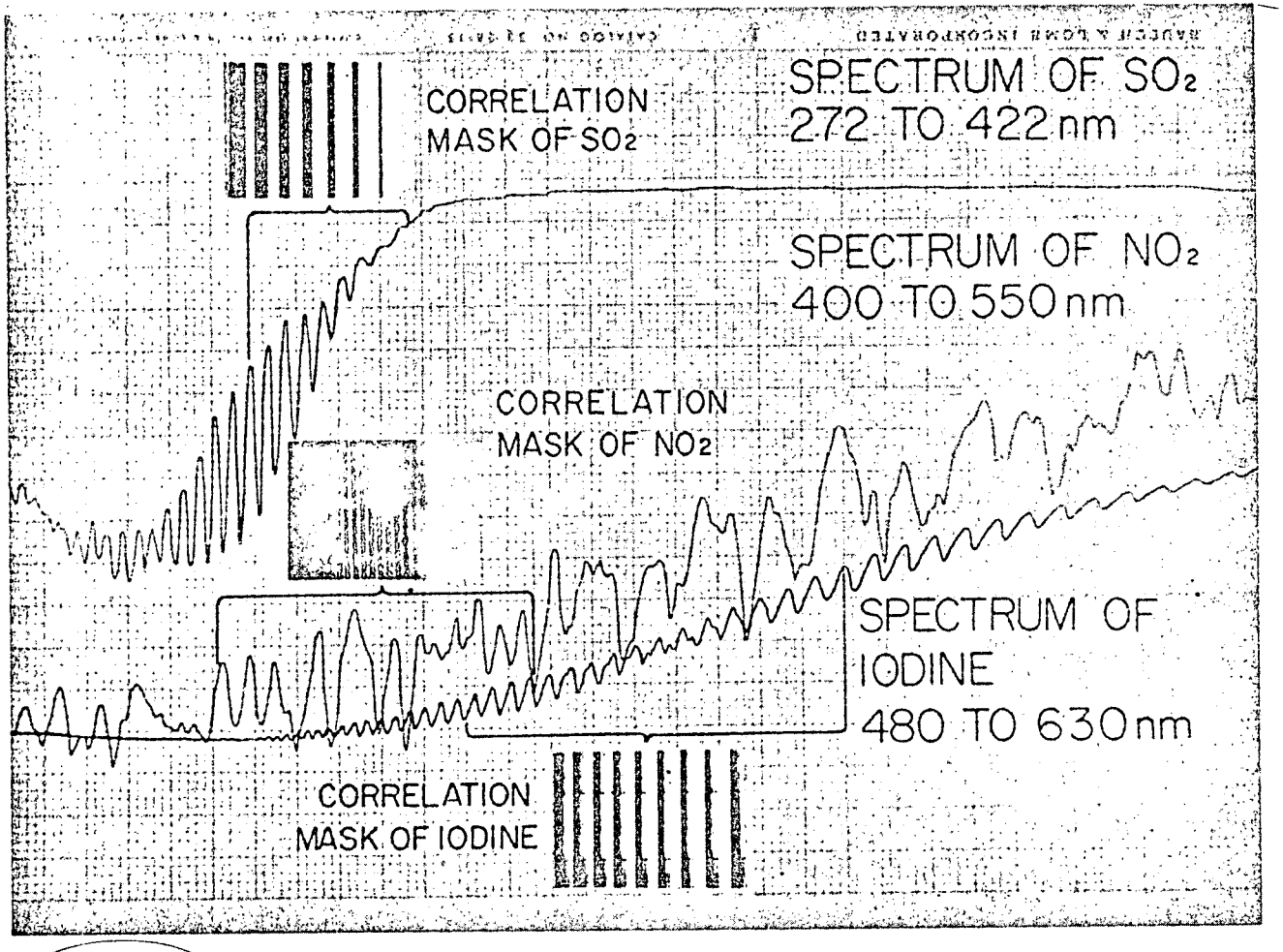
CORRELATION
MASK OF SO2
SPECTRUM OF SO2
272 TO 422nm
SPECTRUM OF NO2
400 TO 550nm
CORRELATION
MASK OF NO2
SPECTRUM OF
IODINE
480 TO 630nm
CORRELATION
MASK OF IODINE

FIGURE 1

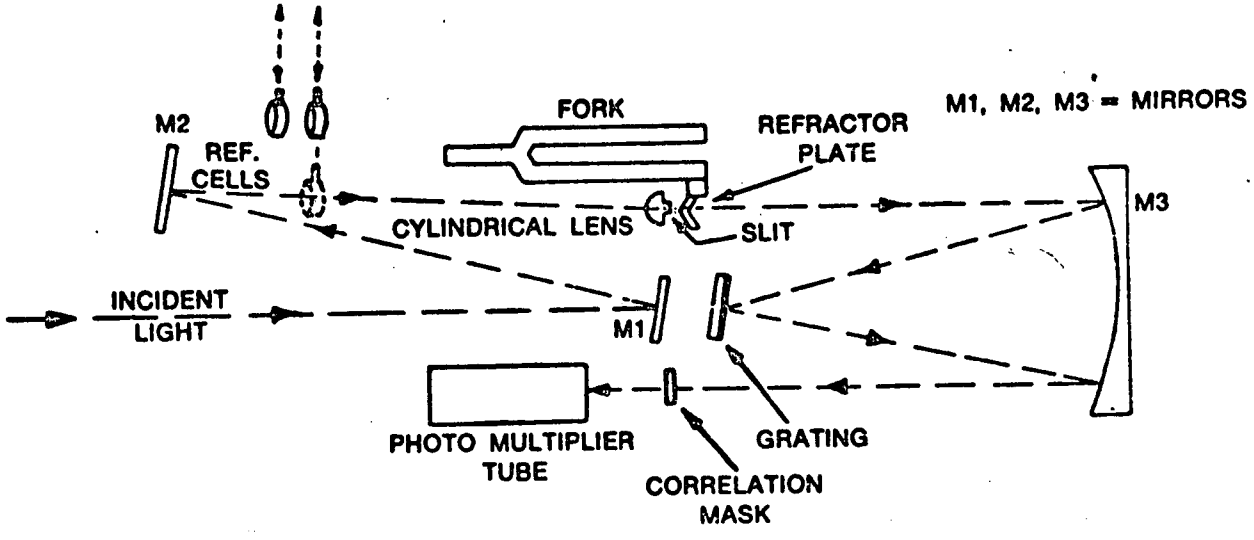

Dispersive system for vapor detection using spectrum correlation filter.

FIGURE 2

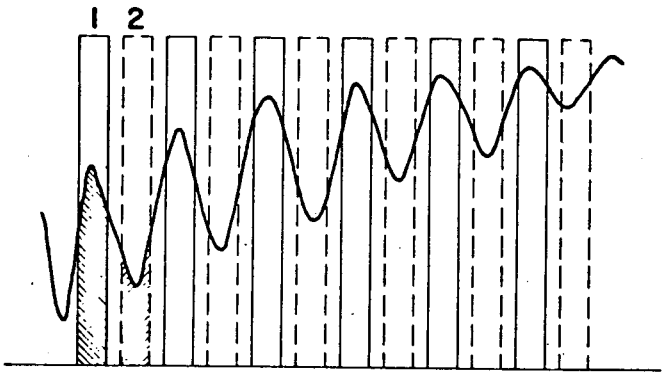

$$M = K \frac{I_o e^{-a_1 c l} - I_o e^{-a_2 c l}}{I_o e^{-a_1 c l}}$$

$$= K \left[1 - \frac{e^{-a_2 c l}}{e^{-a_1 c l}} \right]$$

$$= K \left[1 - e^{-(a_2 - a_1) c l} \right]$$

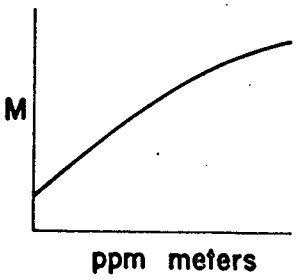

FIGURE 3

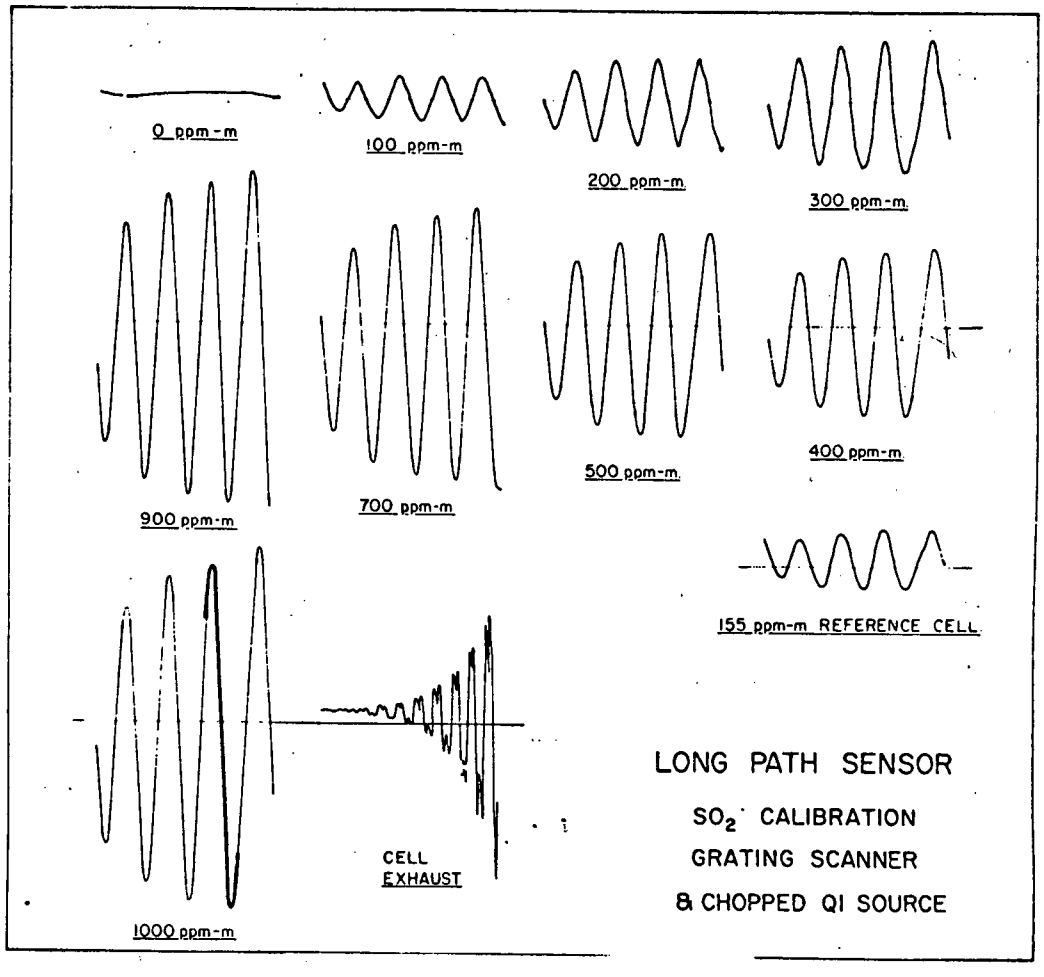
0 ppm-m
100 ppm-m
200 ppm-m
300 ppm-m
900 ppm-m
700 ppm-m
500 ppm-m
400 ppm-m
155 ppm-m REFERENCE CELL
1000 ppm-m
CELL EXHAUST
LONG PATH SENSOR
SO_2 CALIBRATION
GRATING SCANNER
& CHOPPED QI SOURCE

FIGURE 4

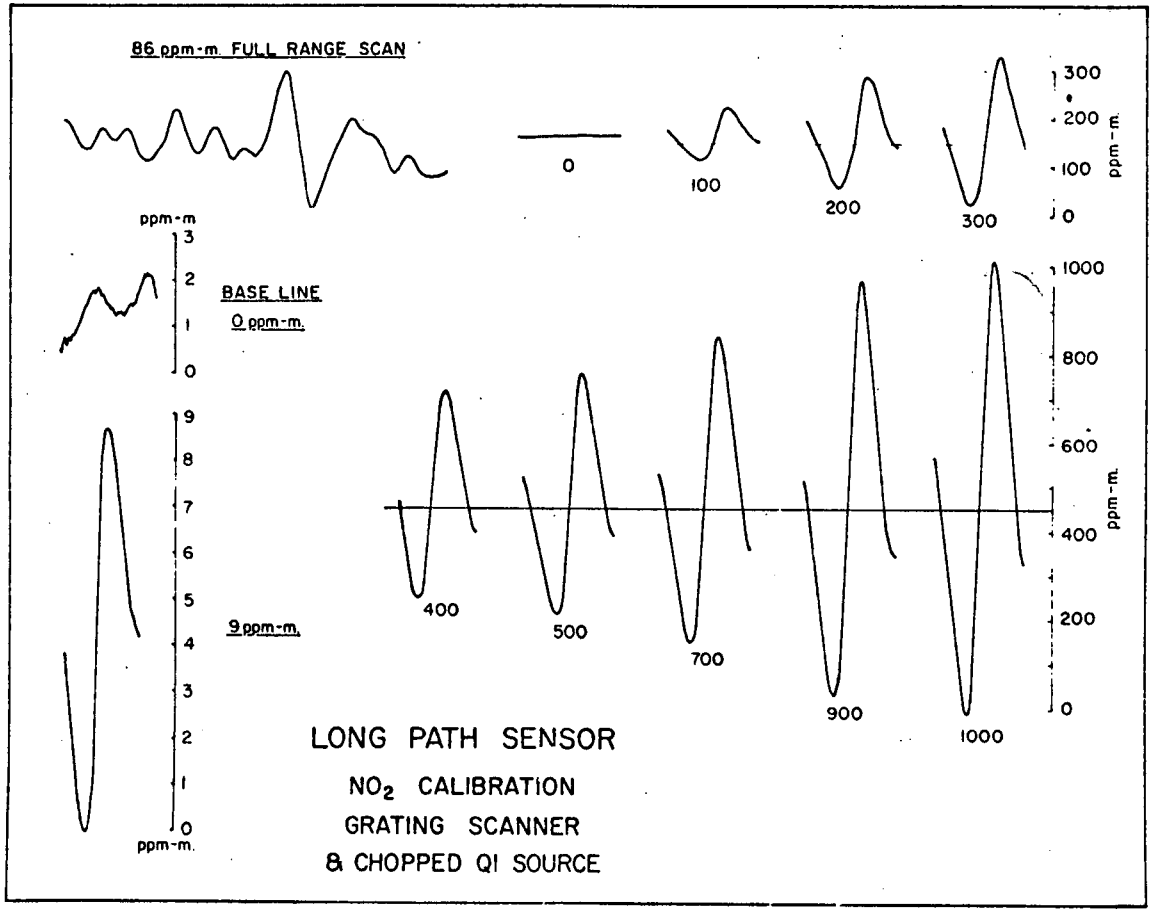
86 ppm-m FULL RANGE SCAN
0
100
200
300
300
200
100
0
ppm-m
ppm-m
3
2
1
0
BASE LINE
0 ppm-m.
1000
800
600
400
200
0
ppm-m.
9
8
7
6
5
4
3
2
1
0
ppm-m.
9 ppm-m.
400
500
700
900
1000
LONG PATH SENSOR
NO2 CALIBRATION
GRATING SCANNER
& CHOPPED QI SOURCE

FIGURE 5

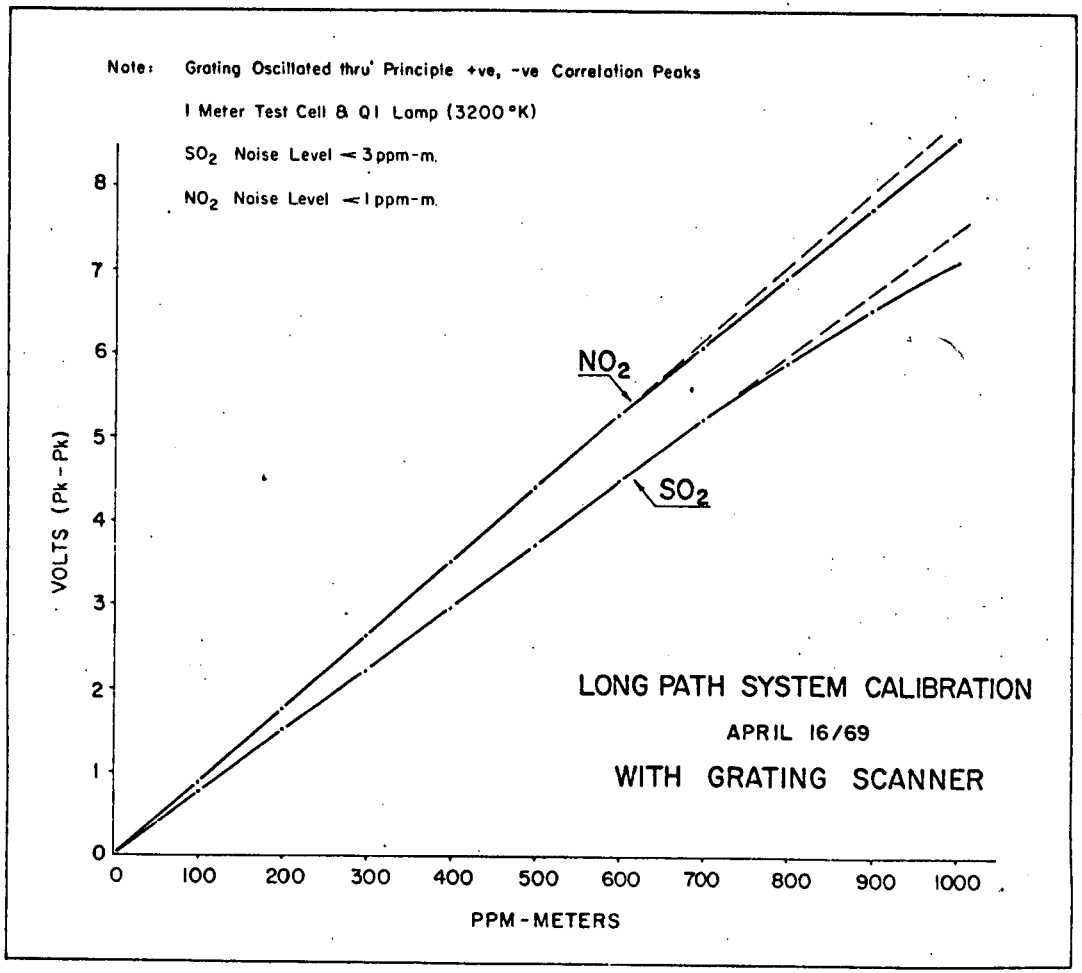
Note: Grating Oscillated thru' Principle +ve, -ve Correlation Peaks
1 Meter Test Cell & Q1 Lamp (3200°K)
SO_2 Noise Level < 3 ppm-m.
NO_2 Noise Level < 1 ppm-m.
VOLTS (Pk-Pk)
0
1
2
3
4
5
6
7
8
0
100
200
300
400
500
600
700
800
900
1000
PPM-METERS
NO_2
SO_2
LONG PATH SYSTEM CALIBRATION
APRIL 16/69
WITH GRATING SCANNER

FIGURE 6

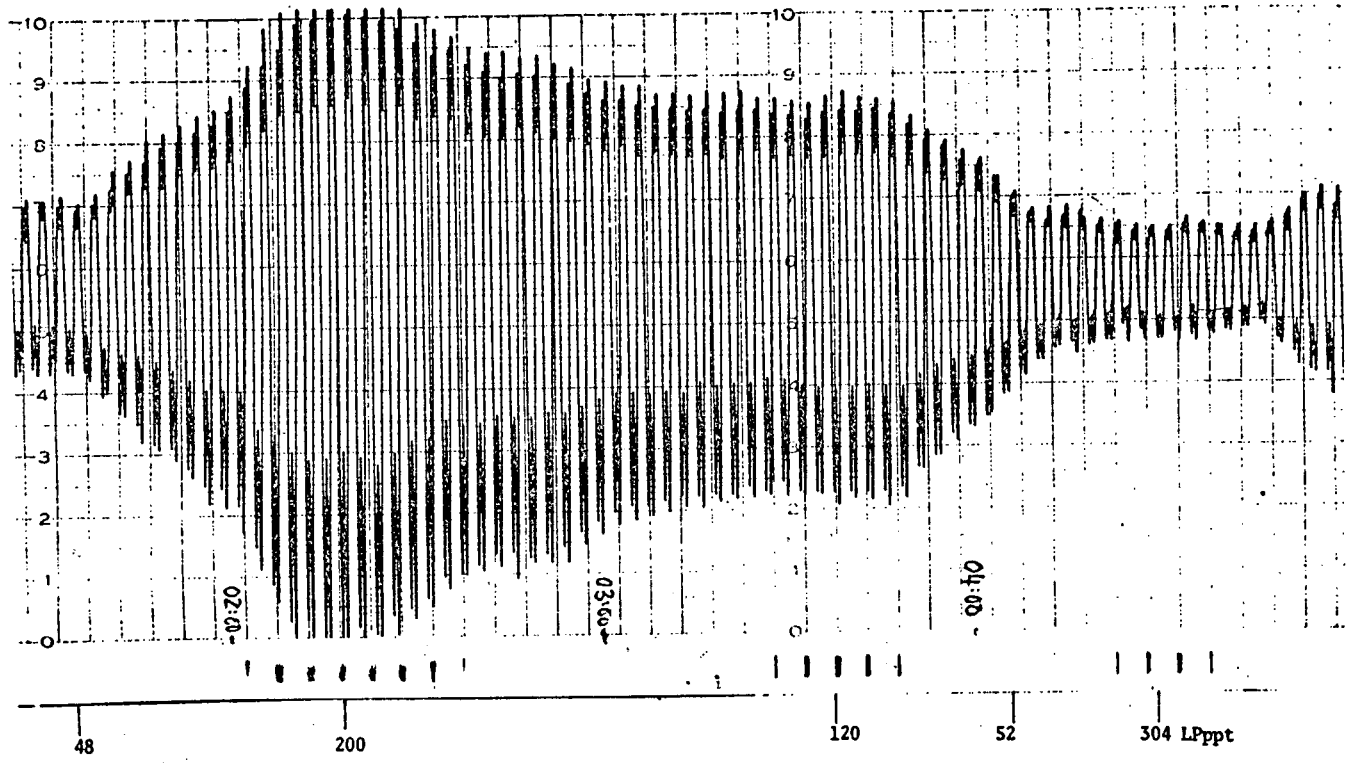

Chart Speed = 3"/hr.
Grating Scan Speed = 15 Å/min.
Grating Scan Interval = 2 min.

SO_2 LONG PATH MONITOR PROFILES

930 METER PATH LENGTH
MAY 15/69

FIGURE 7

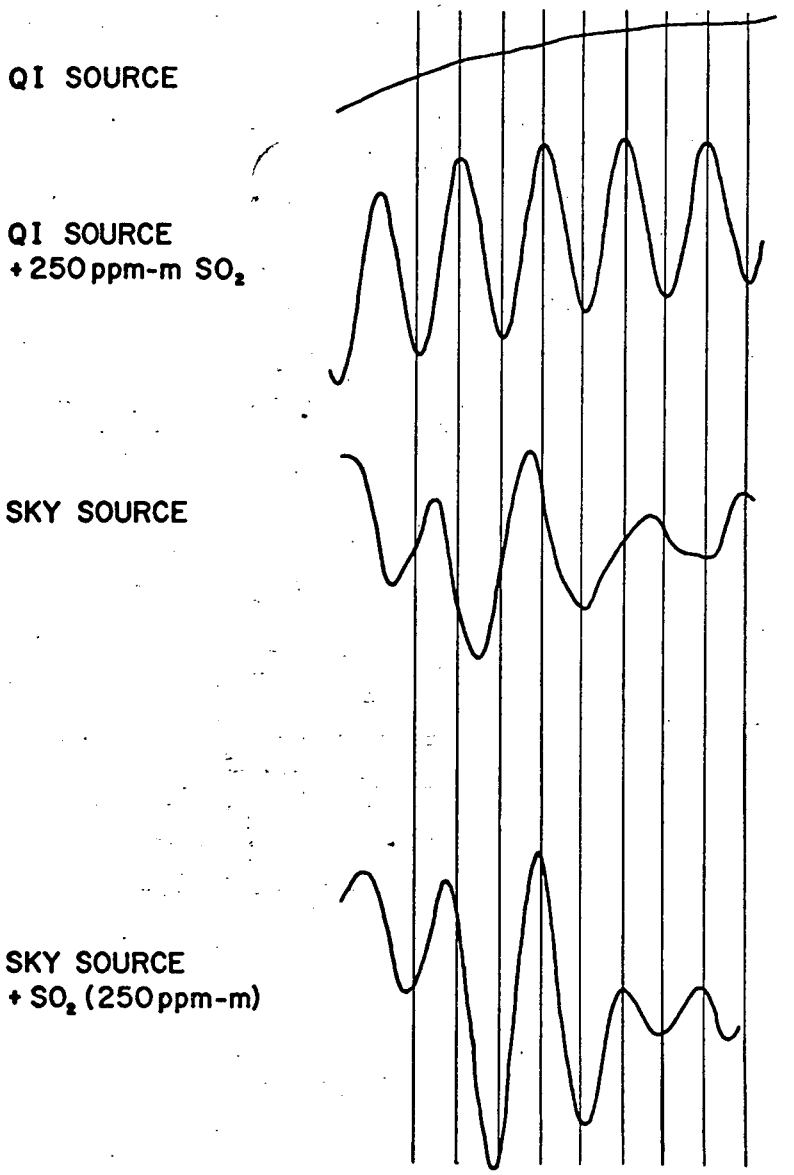

SO_2 CORRELATION SCANS
(SHORT λ)

FIGURE 8

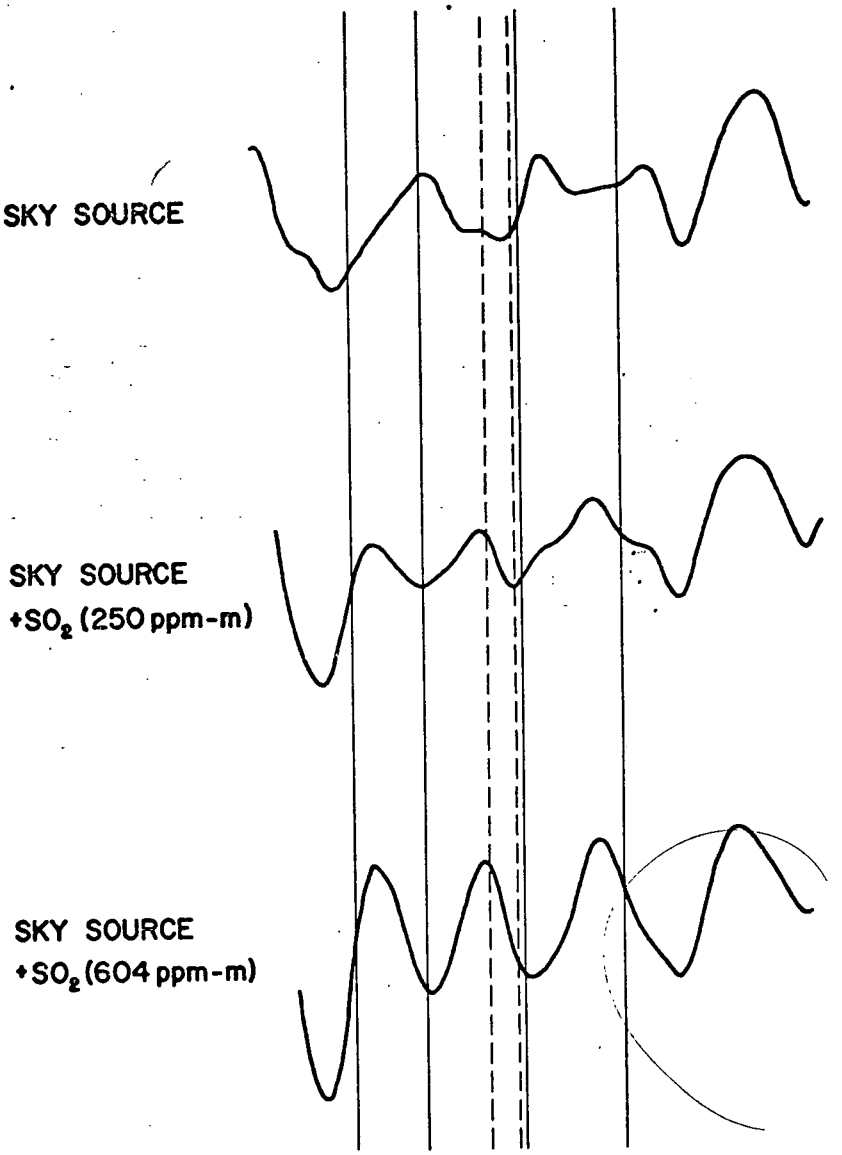

SO₂ CORRELATION SCANS
(LONG λ)

FIGURE 9

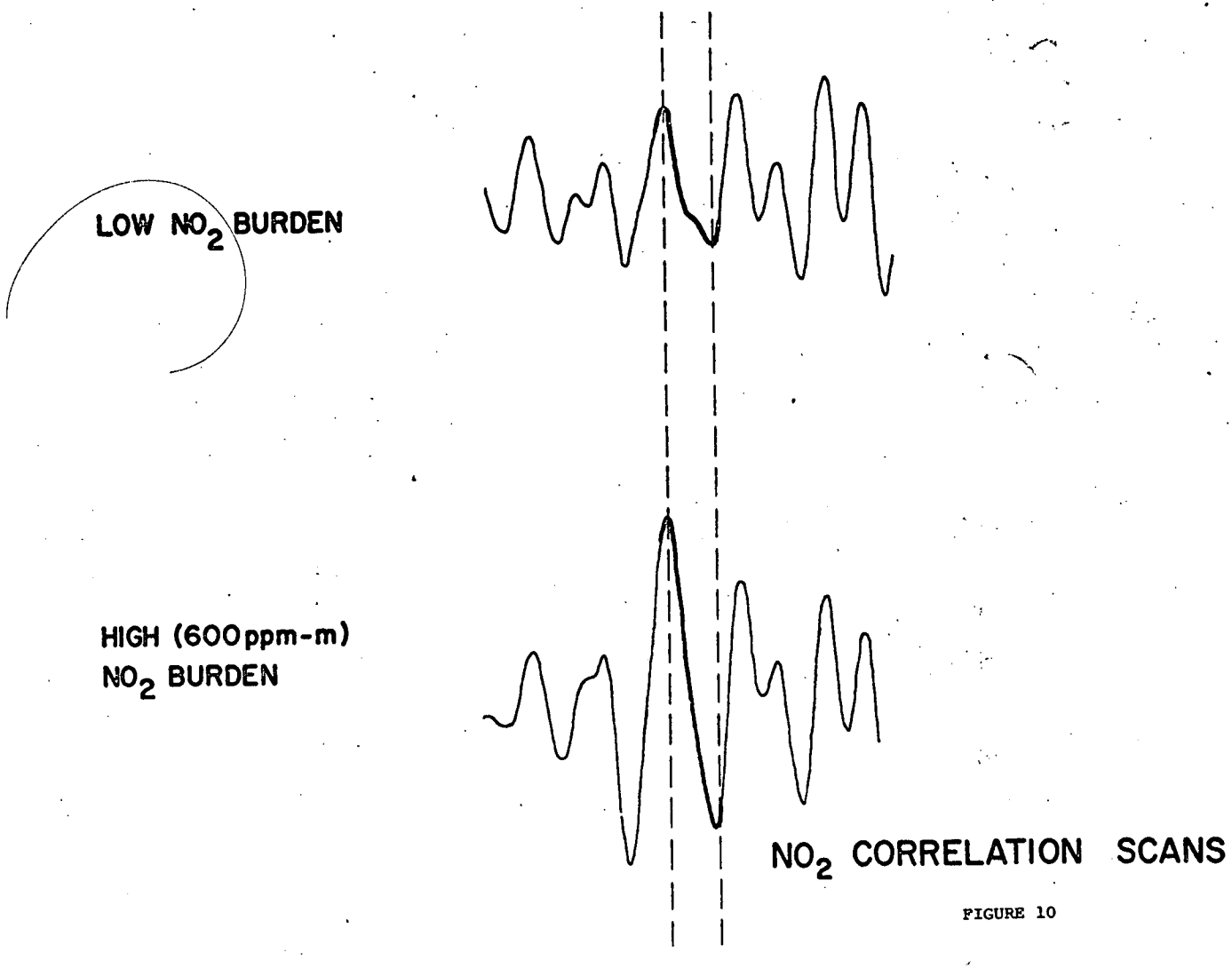

NO_2 CORRELATION SCANS

FIGURE 10

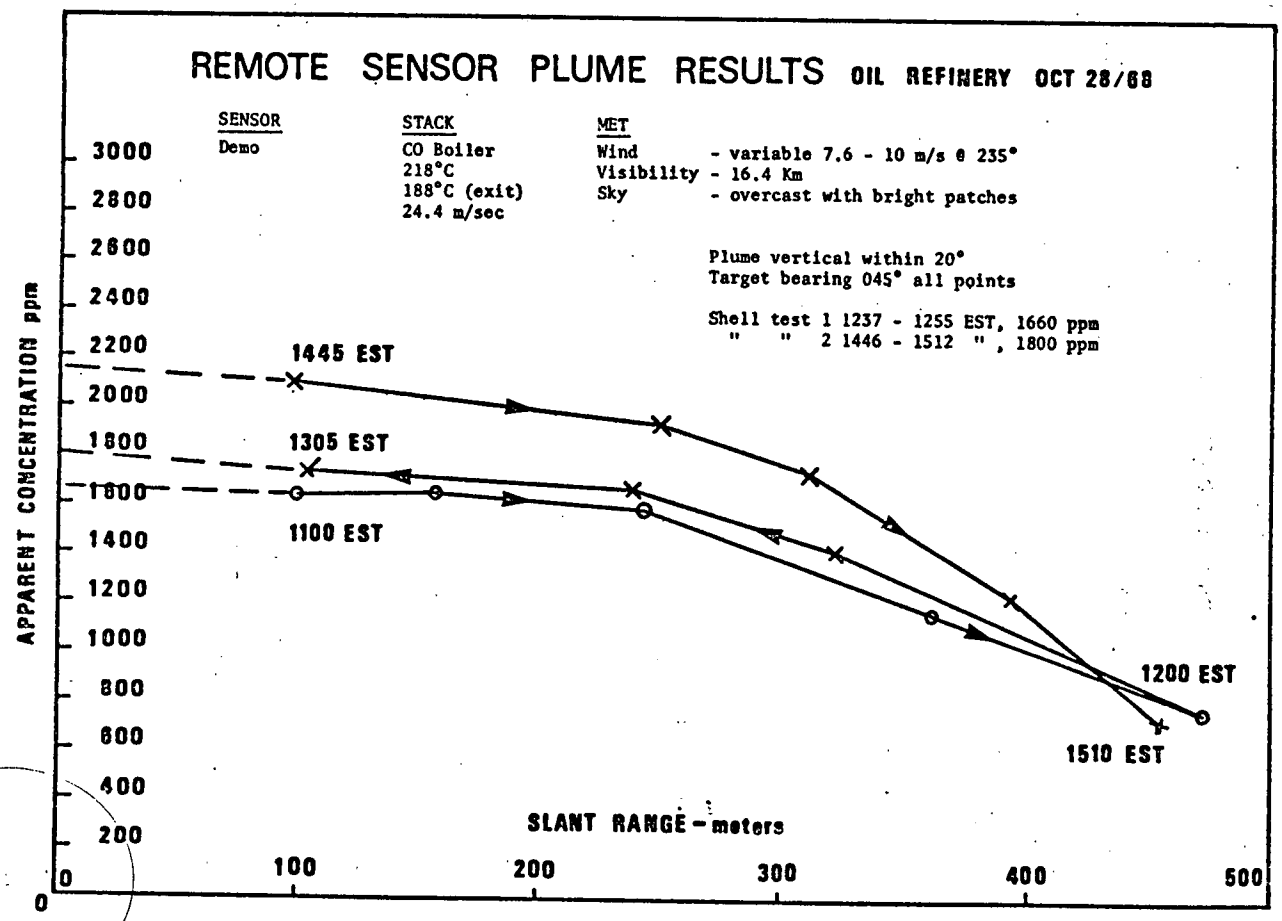
REMOTE SENSOR PLUME RESULTS OIL REFINERY OCT 28/68
SENSOR
Demo
STACK
CO Boiler
218°C
188°C (exit)
24.4 m/sec
MET
Wind - variable 7.6 - 10 m/s @ 235°
Visibility - 16.4 Km
Sky - overcast with bright patches
Plume vertical within 20°
Target bearing 045° all points
Shell test 1 1237 - 1255 EST, 1660 ppm
" " 2 1446 - 1512 " , 1800 ppm
1445 EST
1305 EST
1100 EST
1200 EST
1510 EST
APPARENT CONCENTRATION ppm
SLANT RANGE - meters
0
200
400
600
800
1000
1200
1400
1600
1800
2000
2200
2400
2600
2800
3000
100
200
300
400
500

FIGURE 11

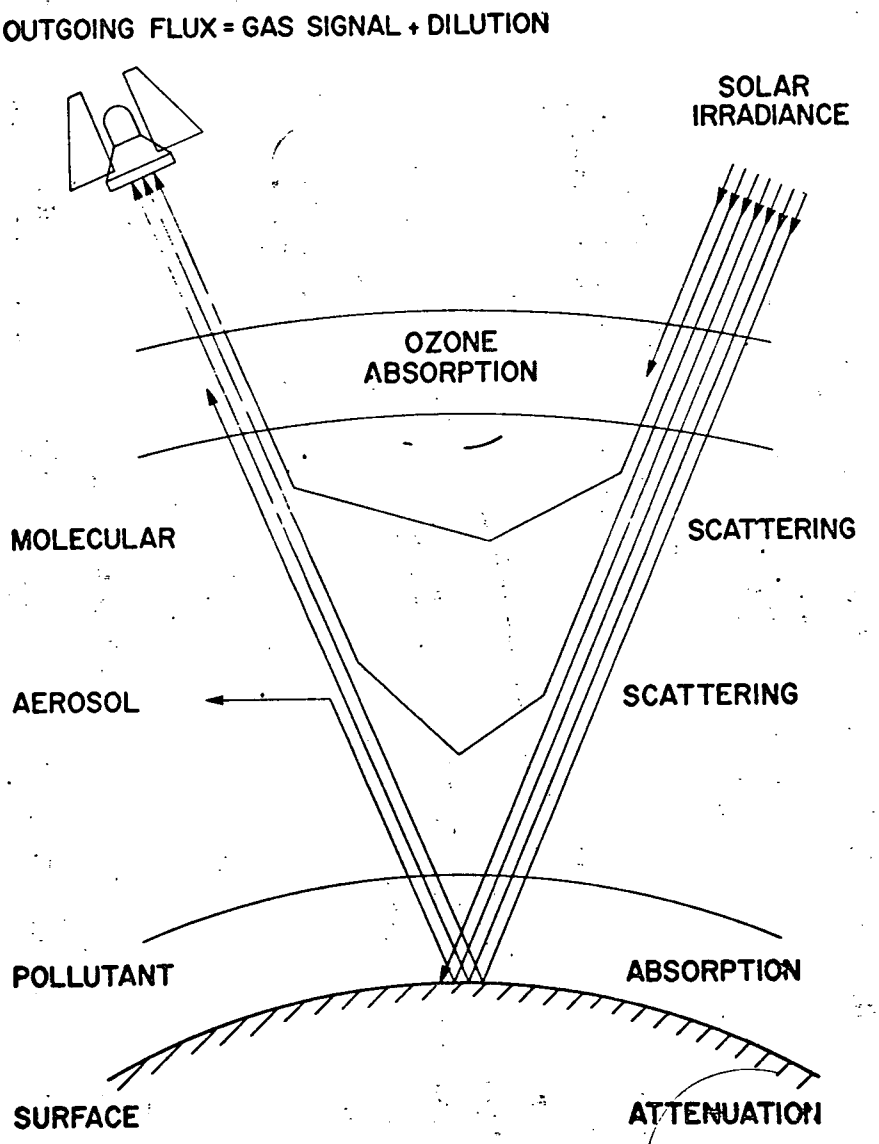

ATTENUATION & DILUTION

FIGURE 12

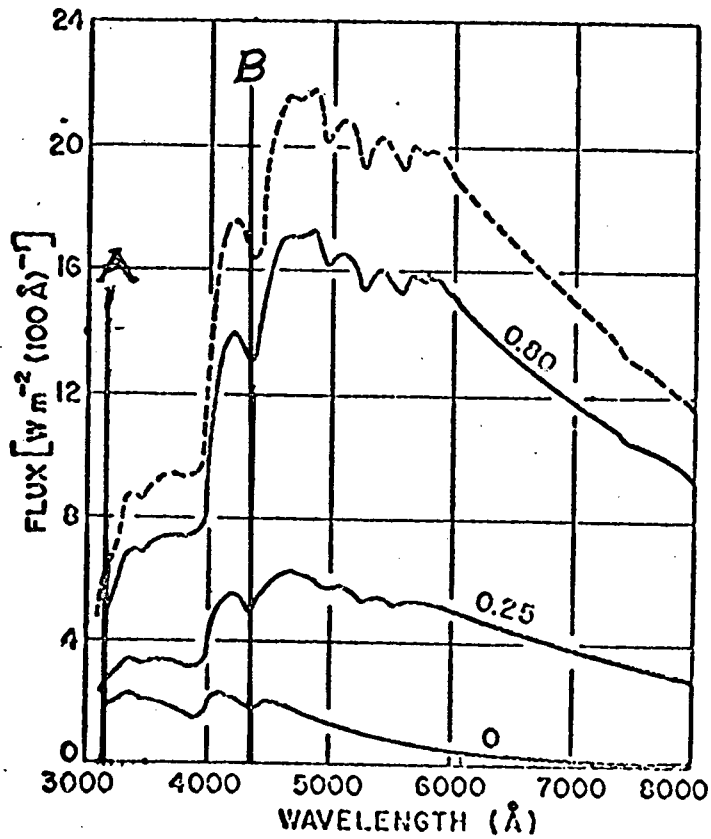

Spectral distribution of flux emerging from top of a model atmosphere for different values of surface reflectance ($r = 0$, 0.25, and 0.80) and the sun at the zenith; dashed curve is the incident extraterrestrial flux. (After Coulson [1959].)

EMERGING FLUX DISTRIBUTION

FIGURE 13

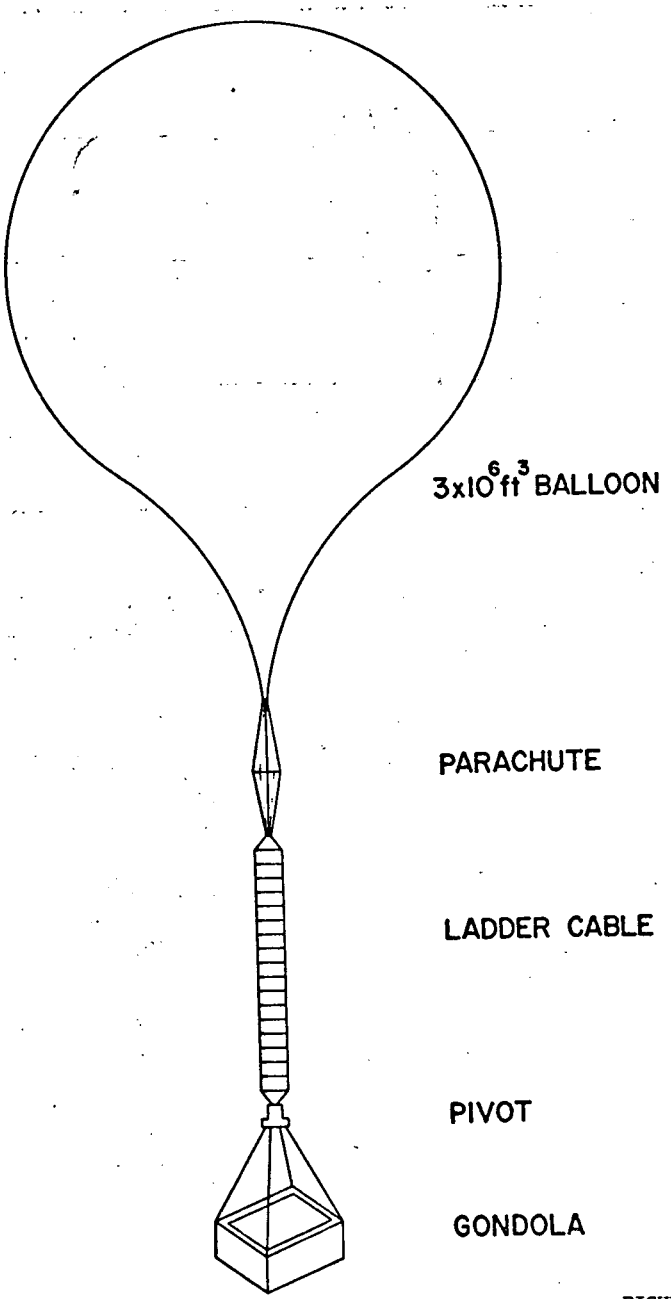

FIGURE 14

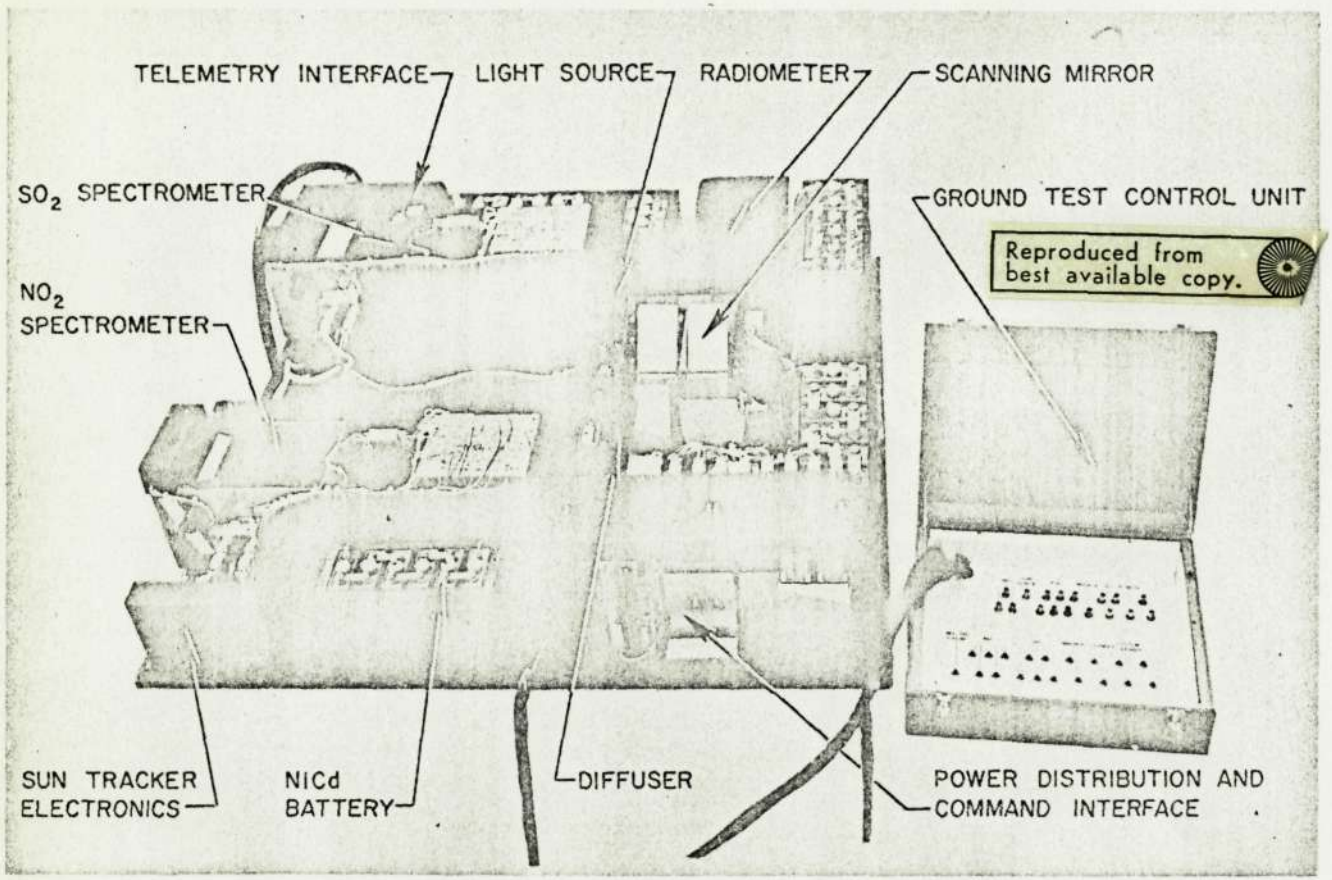

NASA/BARRINGER RESEARCH/NCAR/WINZEN SCIENTIFIC PAYLOAD
FOR HIGH ALTITUDE BALLOON MEASUREMENTS OF AIR POLLUTION

FIGURE 15

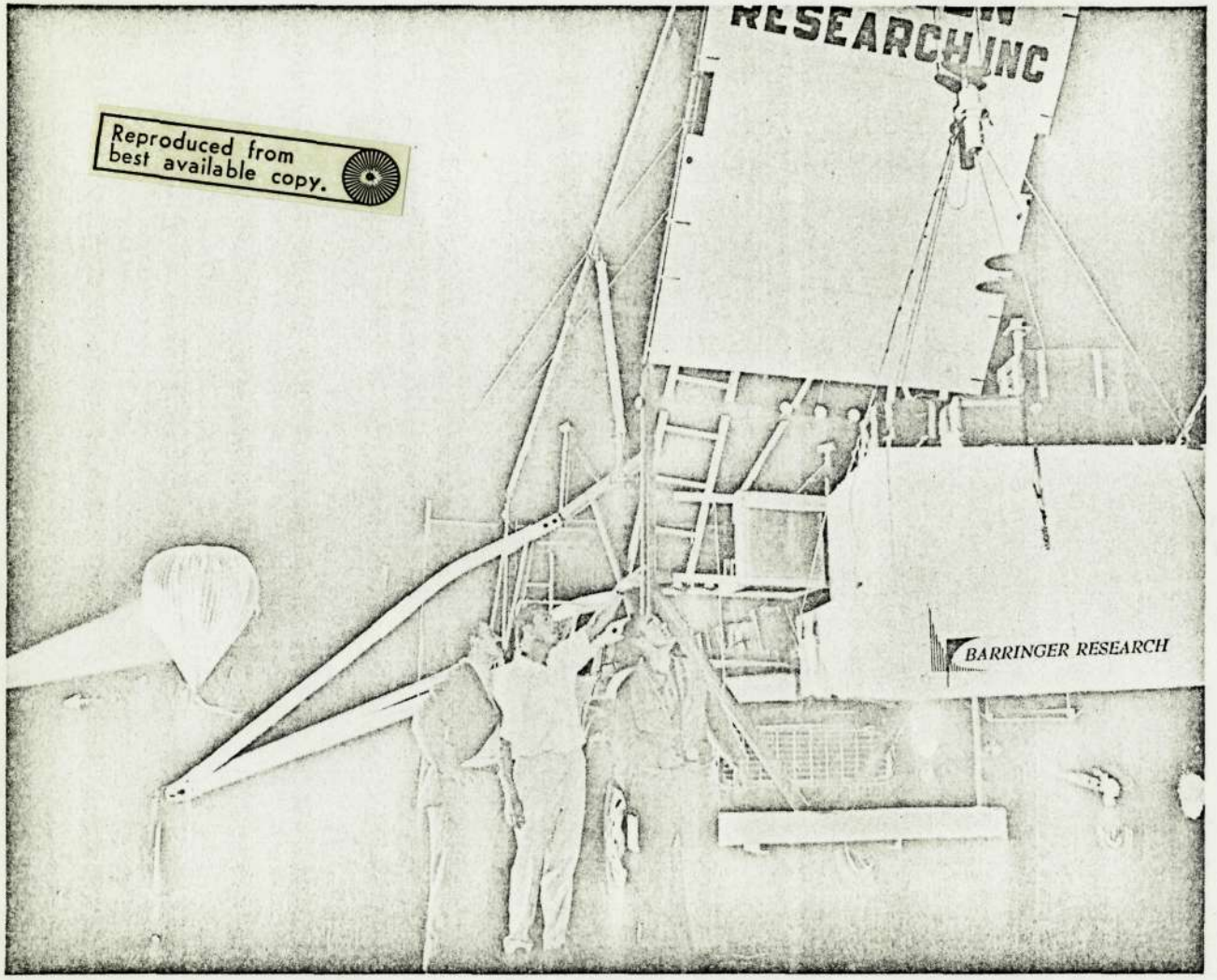

FIGURE 16

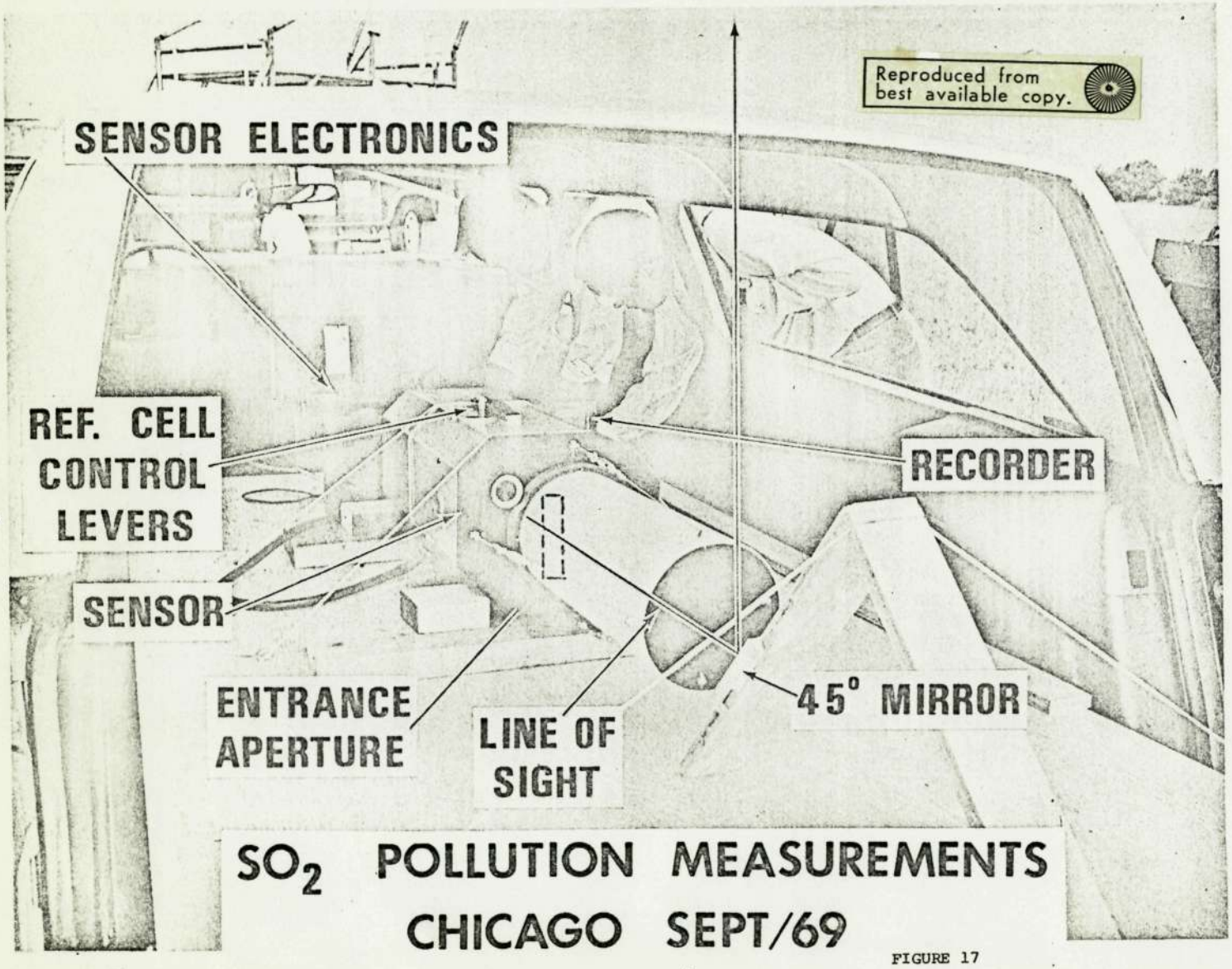
Reproduced from best available copy.
SENSOR ELECTRONICS
REF. CELL CONTROL LEVERS
RECORDER
SENSOR
ENTRANCE APERTURE
LINE OF SIGHT
45° MIRROR
SO2 POLLUTION MEASUREMENTS
CHICAGO SEPT/69

FIGURE 17

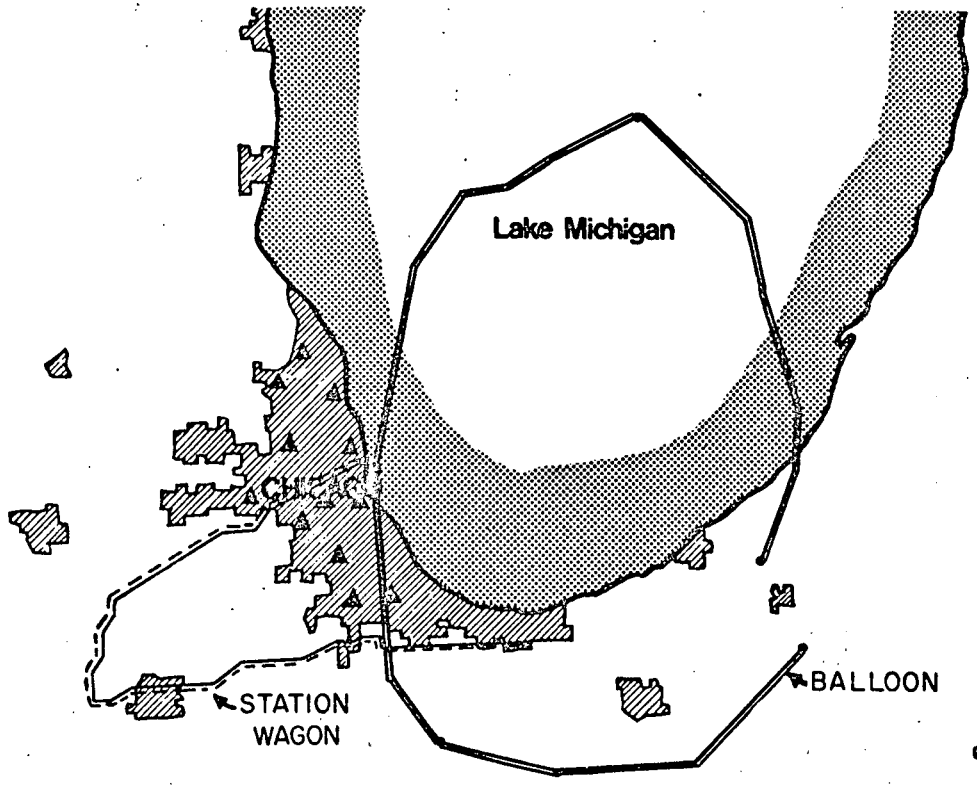

BALLOON TRAJECTORY & STATION WAGON ROUTE

SEPTEMBER 3rd 1969

FIGURE 18

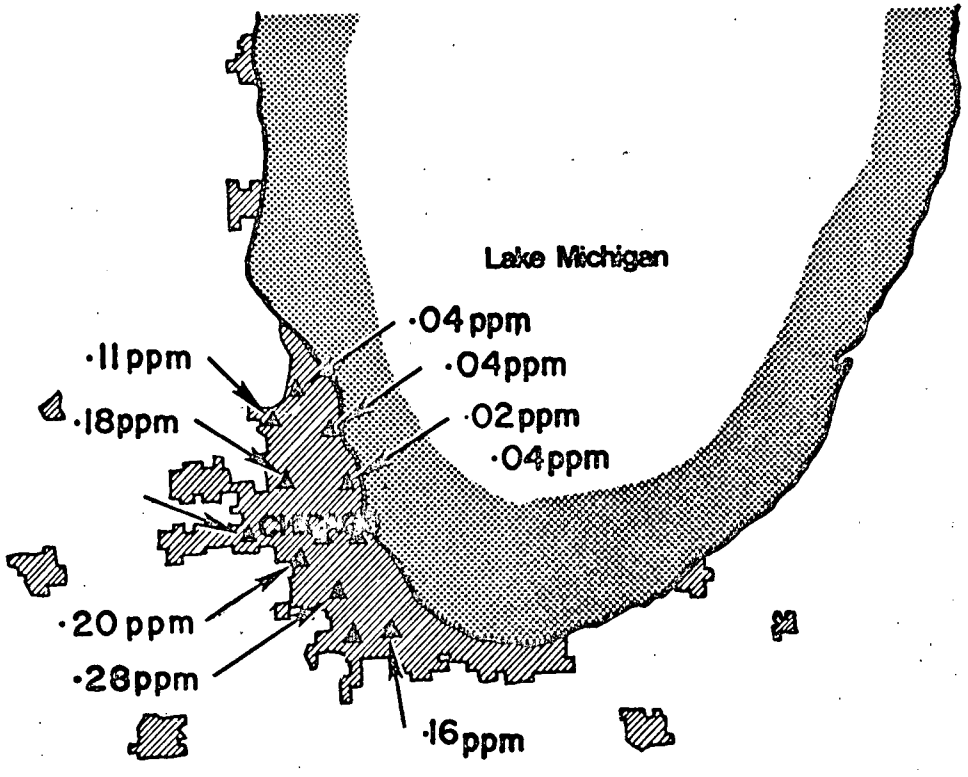

CHICAGO GROUND LEVEL SO_2

1215 CST SEPT. 3rd. 1969

FIGURE 19

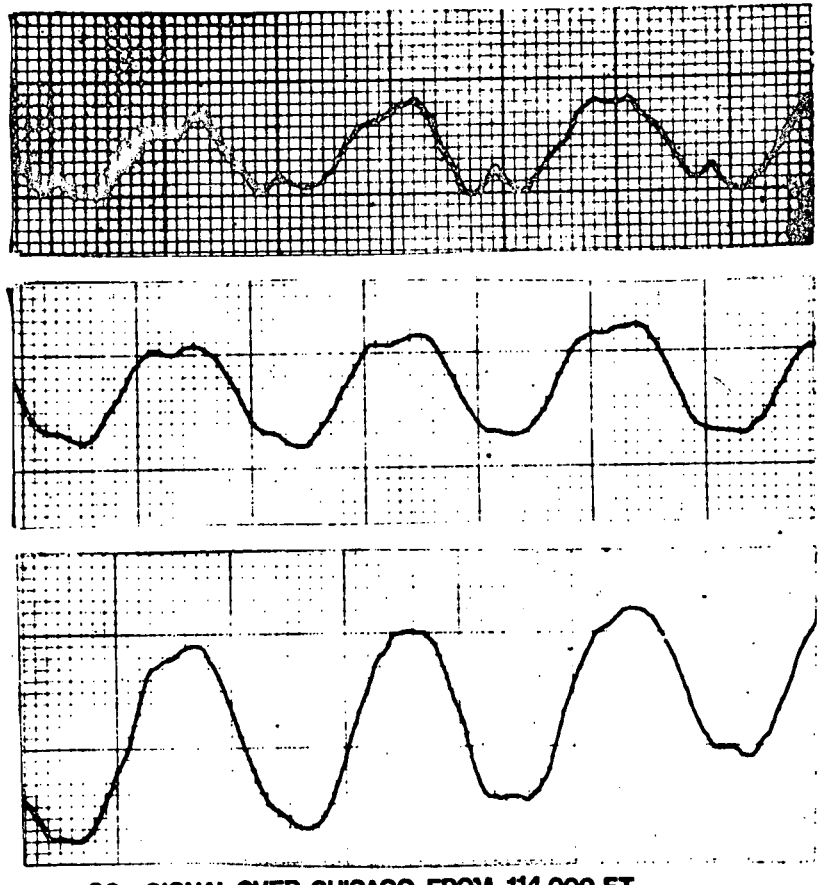

SO_2 SIGNAL OVER CHICAGO FROM 114,000 FT.

FIGURE 20

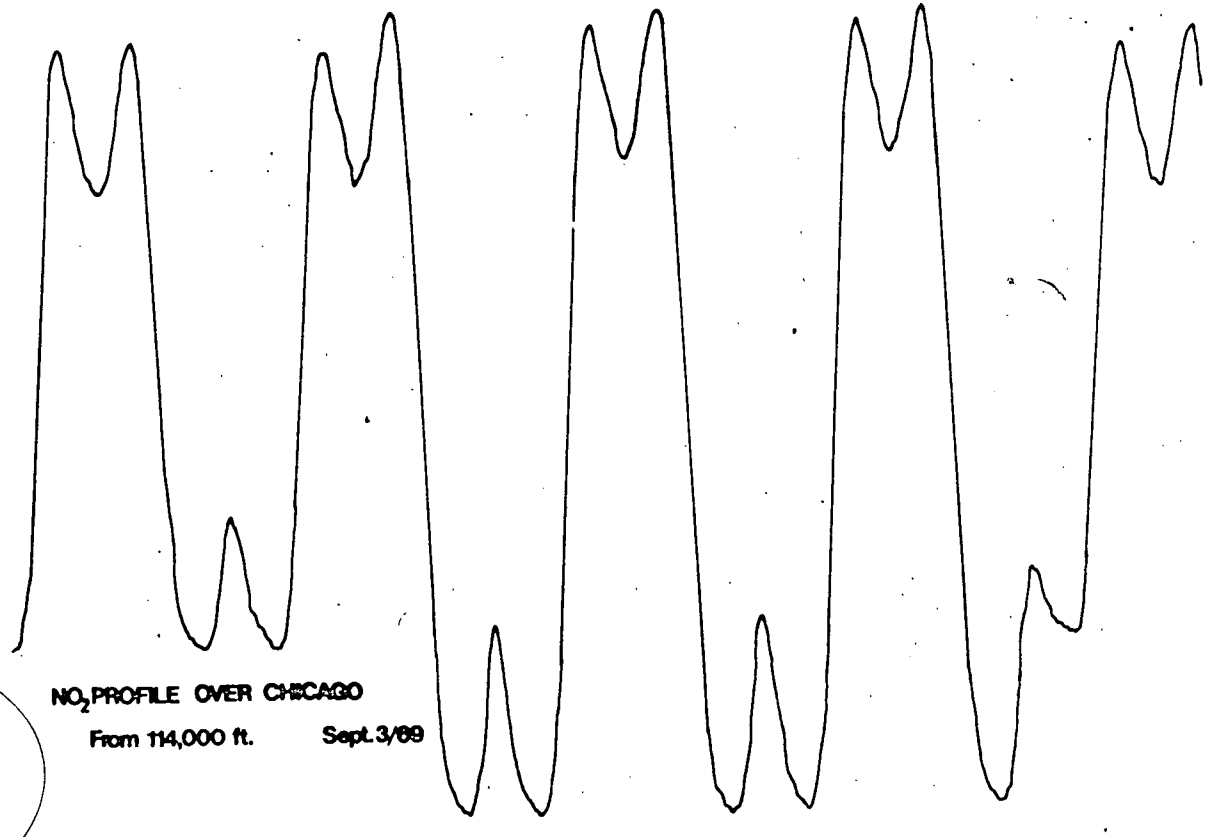

FIGURE 21

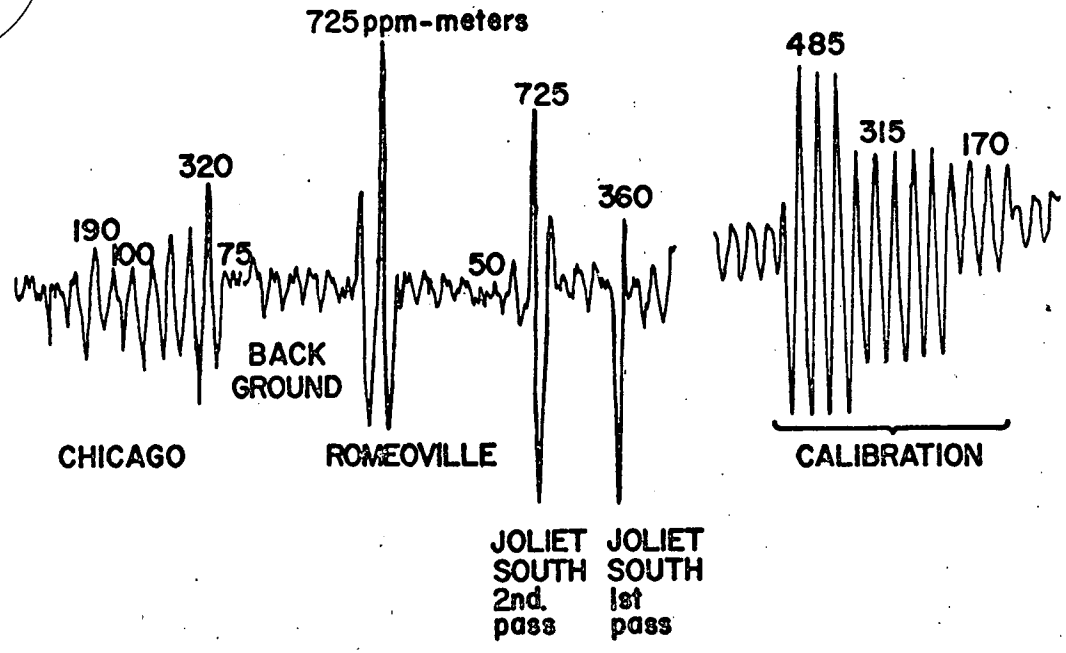

SO_2 VERTICAL PROFILE - GROUND TRAVERSE - CHICAGO

SEPT. 3rd 1969

FIGURE 22

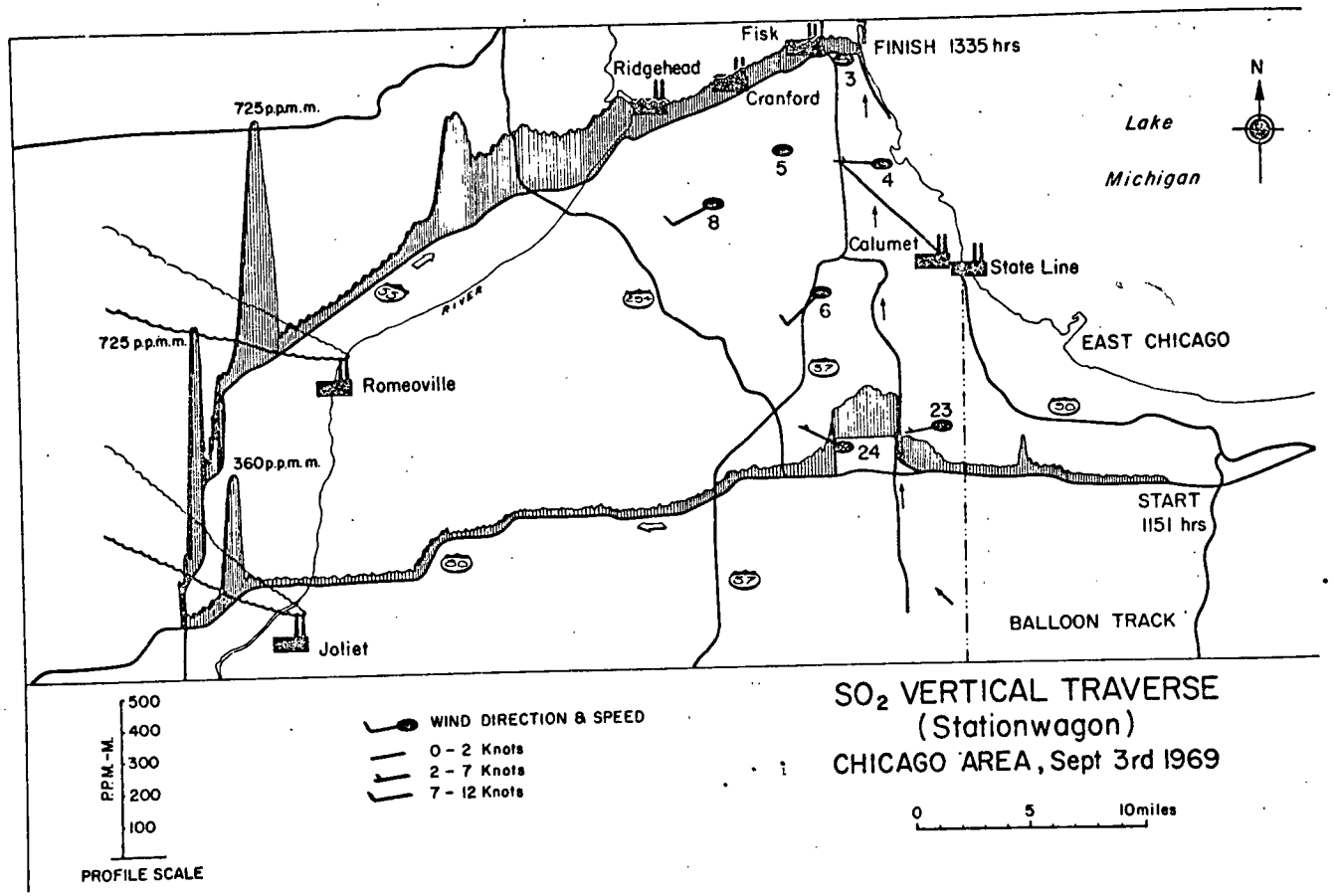
Fisk
FINISH 1335 hrs
Ridgehead
Cranford
725 p.p.m.m.
Lake
Michigan
N
3
4
5
8
Calumet
State Line
6
EAST CHICAGO
725 p.p.m.m.
Romeoville
23
24
360 p.p.m.m.
START
1151 hrs
BALLOON TRACK
Joliet
P.P.M.-M.
500
400
300
200
100
PROFILE SCALE
WIND DIRECTION & SPEED
0 - 2 Knots
2 - 7 Knots
7 - 12 Knots
SO2 VERTICAL TRAVERSE
(Stationwagon)
CHICAGO AREA, Sept 3rd 1969
0
5
10miles

FIGURE 23

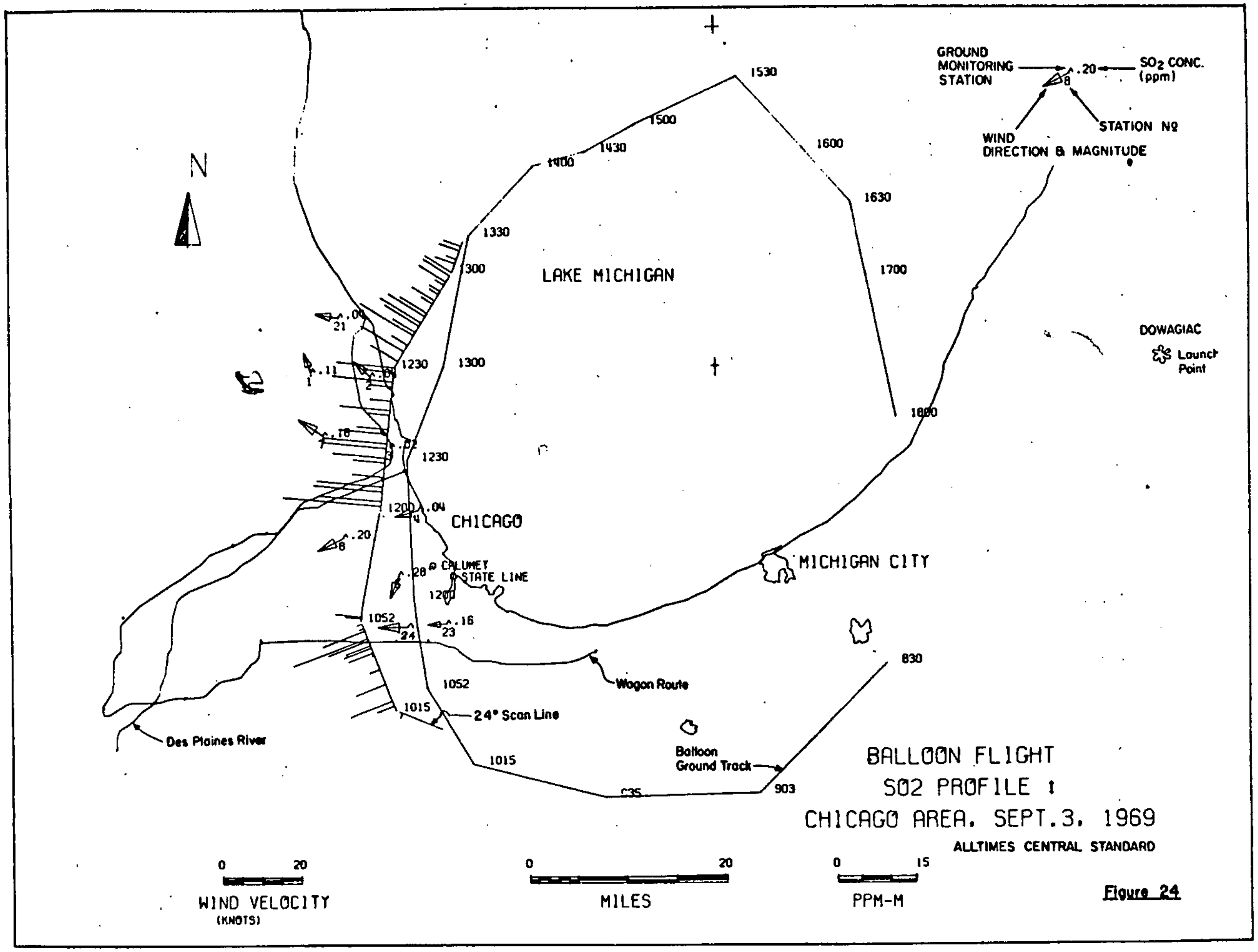

BALLOON FLIGHT
S02 PROFILE 1
CHICAGO AREA, SEPT.3, 1969
ALLTIMES CENTRAL STANDARD

Figure 24

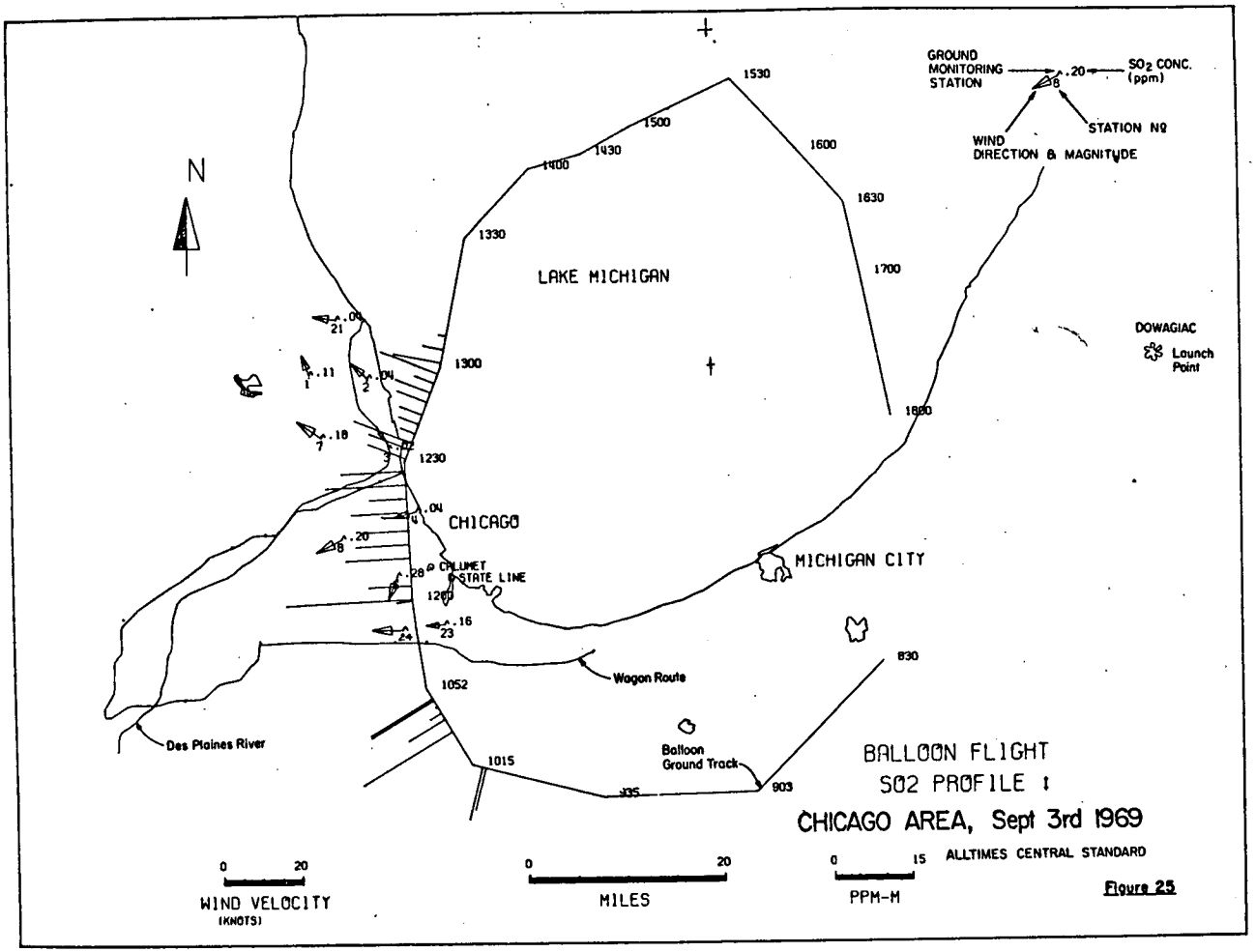
GROUND MONITORING STATION
.20
SO_2 CONC. (ppm)
STATION NO
WIND DIRECTION & MAGNITUDE
N
LAKE MICHIGAN
1530
1500
1430
1400
1600
1630
1700
1800
1330
1300
1230
1200
1052
1015
935
903
830
DOWAGIAC
Launch Point
CHICAGO
CALUMET
STATE LINE
MICHIGAN CITY
Wagon Route
Des Plaines River
Balloon Ground Track
BALLOON FLIGHT
SO2 PROFILE 1
CHICAGO AREA, Sept 3rd 1969
ALLTIMES CENTRAL STANDARD
0 20
WIND VELOCITY (KNOTS)
0 20
MILES
0 15
PPM-M
Figure 25

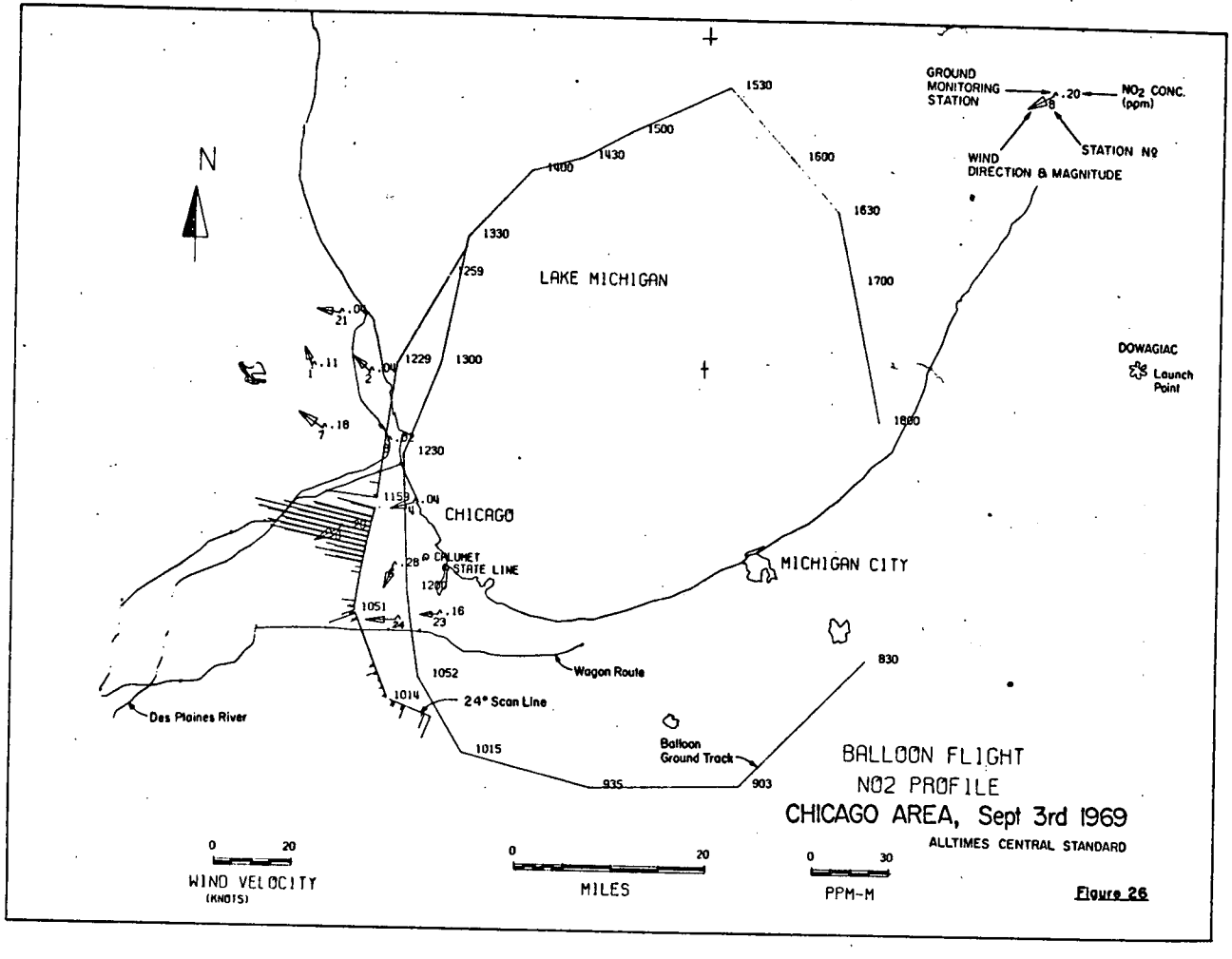
GROUND MONITORING STATION
.20
NO_2 CONC. (ppm)
WIND DIRECTION & MAGNITUDE
STATION NO
N
LAKE MICHIGAN
1530
1500
1430
1400
1600
1630
1330
1259
1700
1229
1300
1880
1230
1159
CHICAGO
CALUMET
STATE LINE
MICHIGAN CITY
1200
1051
1052
1014
1015
935
903
830
Wagon Route
24° Scan Line
Des Plaines River
Balloon Ground Track
DOWAGIAC
Launch Point
BALLOON FLIGHT
NO2 PROFILE
CHICAGO AREA, Sept 3rd 1969
ALLTIMES CENTRAL STANDARD
0 20
WIND VELOCITY (KNOTS)
0 20
MILES
0 30
PPM-M

Figure 26

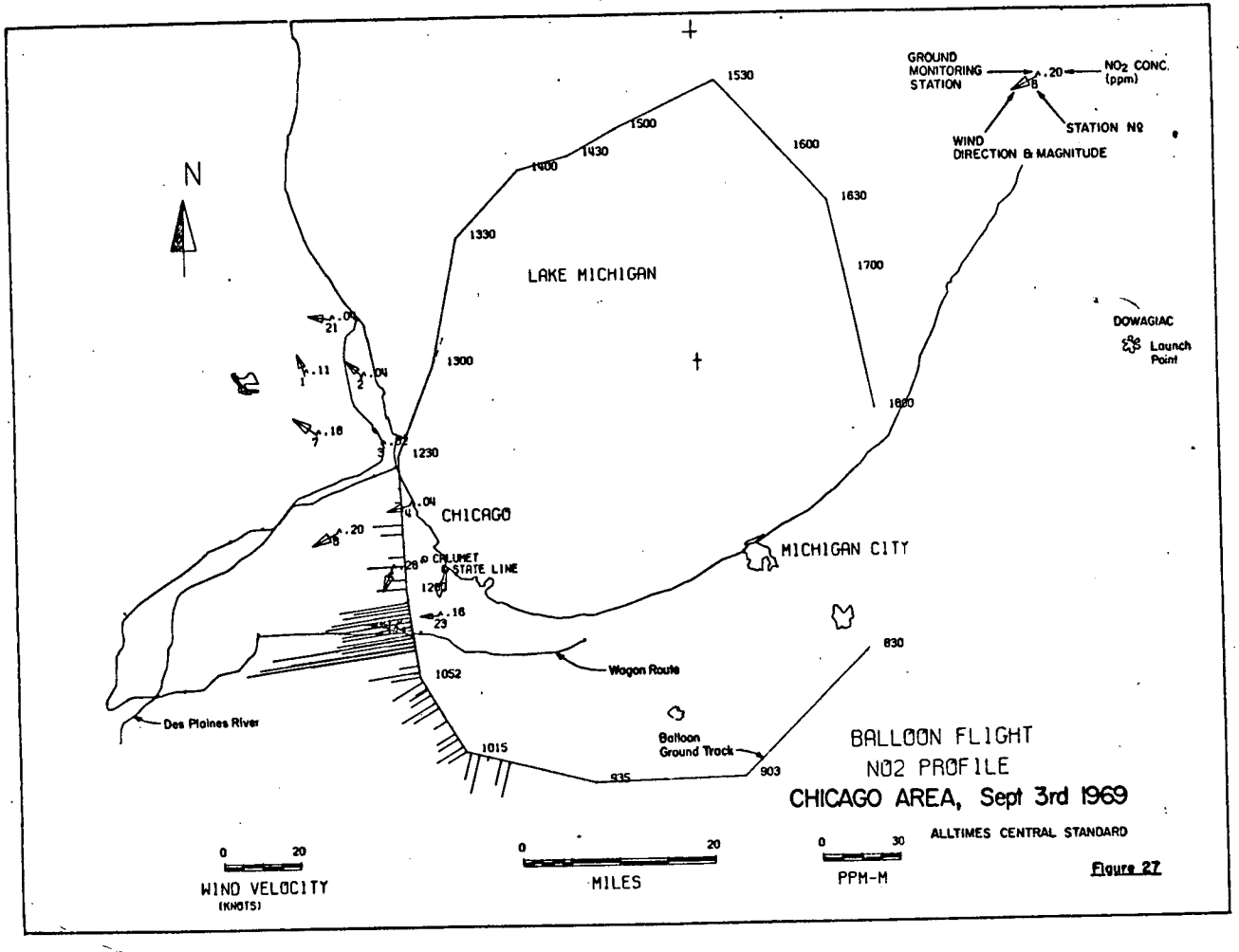
GROUND MONITORING STATION
.20
NO2 CONC. (ppm)
STATION NO
WIND DIRECTION & MAGNITUDE
N
LAKE MICHIGAN
1530
1500
1600
1430
1400
1630
1330
1700
1300
1800
1230
DOWAGIAC
Launch Point
CHICAGO
MICHIGAN CITY
CALUMET STATE LINE
Wagon Route
830
1052
Des Plaines River
Balloon Ground Track
1015
903
935
BALLOON FLIGHT
NO2 PROFILE
CHICAGO AREA, Sept 3rd 1969
ALLTIMES CENTRAL STANDARD
0 20
WIND VELOCITY (KNOTS)
0 20
MILES
0 30
PPM-M

Figure 27